Bioactive Materials 42 (2024) 124–139

Contents lists available at ScienceDirect

Bioactive Materials

journal homepage: www.keaipublishing.com/en/journals/bioactive-materials

Neuroprotection on ischemic brain injury by Mg^{2+}/H_2 released from endovascular Mg implant

Yang Zhang [a,b,1], Hongkang Zhang [c,1], Miaowen Jiang [d,1], Xiaofeng Cao [c], Xiaoxiao Ge [d], Baoying Song [a,b], Jing Lan [d], Wenhao Zhou [e], Zhengfei Qi [d], Xuenan Gu [f], Juzhe Liu [g], Yufeng Zheng [c,***], Ming Li [a,b,**], Xunming Ji [a,b,d,*]

[a] Department of Neurology and Neurosurgery, Xuanwu Hospital, Capital Medical University, Beijing, 100053, China
[b] China-America Institute of Neuroscience and Beijing Institute of Geriatrics, Xuanwu Hospital, Capital Medical University, Beijing, 100053, China
[c] School of Materials Science and Engineering, Peking University, Beijing, 100871, China
[d] Beijing Institute for Brain Disorders, Capital Medical University, Beijing, 100069, China
[e] Biomaterials Research Center, Northwest Institute for Non-ferrous Metal Research, Xi'an, 710016, China
[f] School of Bioengineering, Beihang University, Beijing, 100191, China
[g] The Key Laboratory of Resources and Environmental System Optimization, Ministry of Education, College of Environmental Science and Engineering, North China Electric Power University, Beijing, 100096, China

ARTICLE INFO

Keywords:
Magnesium
Acute ischemic stroke
Neuroprotection
Biodegradable implantation
Hydrogen

ABSTRACT

Most acute ischemic stroke patients with large vessel occlusion require stent implantation for complete recanalization. Yet, due to ischemia-reperfusion injury, over half of these patients still experience poor prognoses. Thus, neuroprotective treatment is imperative to alleviate the ischemic brain injury, and a proof-of-concept study was conducted on "biodegradable neuroprotective stent". This concept is premised on the hypothesis that locally released Mg^{2+}/H_2 from Mg metal within the bloodstream could offer synergistic neuroprotection against reperfusion injury in distant cerebral ischemic tissues. Initially, the study evaluated pure Mg's neuroactive potential using oxygen-glucose deprivation/reoxygenation (OGD/R) injured neuron cells. Subsequently, a pure Mg wire was implanted into the common carotid artery of the transient middle cerebral artery occlusion (MCAO) rat model to simulate human brain ischemia/reperfusion injury. *In vitro* analyses revealed that pure Mg extract aided mouse hippocampal neuronal cell (HT-22) in defending against OGD/R injury. Additionally, the protective effects of the Mg wire on behavioral abnormalities, neural injury, blood-brain barrier disruption, and cerebral blood flow reduction in MCAO rats were verified. Conclusively, Mg-based biodegradable neuroprotective implants could serve as an effective local Mg^{2+}/H_2 delivery system for treating distant cerebral ischemic diseases.

1. Introduction

The quest for effective neuroprotection on acute ischemic stroke (AIS) has long plagued clinicians [1–3]. Due to the ischemia/reperfusion (I/R) injury, over half of these patients continue to face poor prognosis after the recanalization therapy [4]. Among them, intracranial atherosclerosis-induced large vessel occlusion accounts for 15–35 % of AIS cases [5], with most patients requiring stent implantation post-thrombectomy for complete recanalization. Therefore, integrating recanalization therapy with neuroprotective treatments to alleviate I/R injury is essential. Biodegradable Mg metals, capable of producing and releasing neuroprotective agents like magnesium ions and hydrogen molecules, are promising candidate materials to make neuroprotective brain stent.

Peer review under responsibility of KeAi Communications Co., Ltd.
* Corresponding author. Department of Neurology and Neurosurgery, Xuanwu Hospital, Capital Medical University, Beijing, 100053, China.
** Corresponding author. China-America Institute of Neuroscience and Beijing Institute of Geriatrics, Xuanwu Hospital, Capital Medical University, Beijing, 100053, China.
*** Corresponding author. School of Materials Science and Engineering, Peking University, Beijing, 100871, China.
E-mail addresses: yfzheng@pku.edu.cn (Y. Zheng), liming@xwhosp.org (M. Li), jixm@ccmu.edu.cn (X. Ji).
[1] These authors contributed equally to this work.

https://doi.org/10.1016/j.bioactmat.2024.08.019
Received 1 July 2024; Received in revised form 10 August 2024; Accepted 19 August 2024

Magnesium ion supplementation can reduce cerebral ischemia via three primary mechanisms: reducing intracellular calcium overload, enhancing cerebral blood flow, and sustaining energy metabolism post-cerebral ischemia [6]. Direct infusion of Mg^{2+} into target organs through proximal arteries can amplify their neuroprotective effects [7] and minimize blood-brain barrier damage [8]. Furthermore, hydrogen gas has been identified as a neuroprotective therapeutic agent, safeguarding against oxidative harm [9–11]. Influenced by Shigeo Ohta's pivotal 2007 study [9], H_2 administration through inhalation, injection/infusion, and ingestion has demonstrated significant therapeutic potential for various brain disorders, including I/R injury, traumatic injury, and subarachnoid hemorrhage [11,12]. The safety and efficacy of molecular hydrogen have been explored in patients with ischemic strokes [13–16]. Given its high hydrogen production capacity (41.7 mmol/g), significantly surpassing that of hydrogen-rich saturated water (0.8 μmol/mL), Mg can serve as a long-term hydrogen source [17]. Moreover, a recent clinical trial suggests that the combination therapy of Mg^{2+} and hydrogen has a synergistic protective effect on cerebral disease [18]. Hence, Mg-based cerebrovascular implants could act as localized Mg^{2+} and H_2 delivery systems, treating remote neurological damage in AIS patient after reperfusion.

Magnesium and its alloys, explored extensively as biodegradable cardiovascular stents (such as DREAMS and DREAMS 2G stents) [19,20], have shown promise in BIOSOLVE-I [19] and BIOSOLVE-II [20] clinical trials. These findings have opened new research pathways for Mg-based alloys as cerebrovascular stent implants. However, there

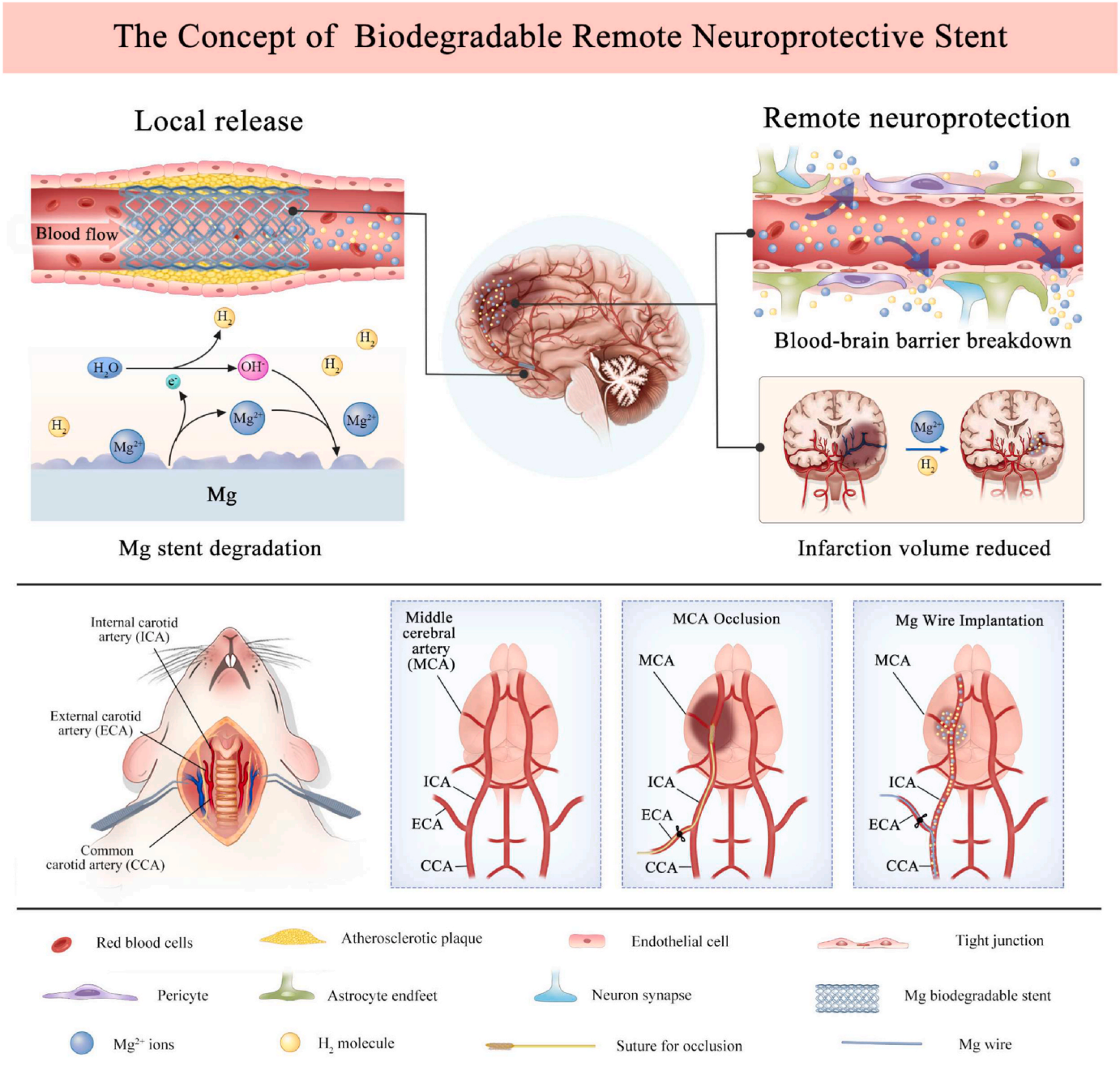

Fig. 1. The proof-of-concept of the biodegradable neuroprotective stent and the implementation strategies to validate this concept. Biodegradable neuroprotective stent refers to stents that could locally produce neuroprotective substances (like Mg^{2+}/H_2) during the degradation of stents within blood flow to the damaged brain tissue, thereby rescuing distal cerebral ischemic tissues. To verify this concept, a middle cerebral artery occlusion rat model was employed, implanting an Mg wire representing Mg stent in the common carotid artery.

remains uncertainty regarding the neurological impacts of Mg degradation products. In one study, a bare Mg-Nd-Zn-Zr stent was implanted in the common carotid artery of healthy New Zealand white rabbits for 20 months, with no observed Mg^{2+} ion accumulation in major organs, including the brain [21]. In addition, an *in vivo* study involved subcutaneous implantation of Mg-Zn alloy plates in rats to examine Mg^{2+} homeostasis within 24 h, revealing no elevated Mg^{2+} levels in healthy rat brains [22]. Nonetheless, given the compromised blood-brain barrier in pathological conditions, the potential effects of Mg implant degradation products in blood vessels on distant ischemic brain tissues remain uncertain.

In this study, we introduced the innovative concept of a "biodegradable neuroprotective stent" and hypothesized that locally released Mg^{2+}/H_2 from Mg metal within blood flow could synergistically protect remote cerebral ischemic tissues. The scientific premises and implementation plan for this study are depicted in Fig. 1. To test this hypothesis, the corrosion behavior of Mg wire in the common carotid artery (CCA) under blood flow was simulated through computational modeling. Subsequently, healthy and oxygen-glucose deprivation/reoxygenation (OGD/R) injured neuron cells were cultured in Mg extract to assess its *in vitro* cytocompatibility and neuroprotective characteristics. Finally, pure Mg wires were implanted in the CCA of the middle cerebral artery occlusion (MCAO) rat model to investigate the underlying neuroprotection mechanisms and *in vivo* corrosion behavior. The impact of Mg wires on behavior, neurorescue, blood-brain barrier (BBB) integrity, and cerebral blood flow recovery were evaluated. Additionally, the time-dependent effects of Mg wire implantation on ion and molecule concentrations in blood and brain tissue were further examined.

2. Results

2.1. Computational modelling of Mg wire corrosion within CCA

Prior to any experimental procedures, assessing the corrosion behavior and the time-dependent release of Mg^{2+} and H_2 from the Mg wire implanted in the CCA was imperative. Fig. 2A displayed the modeling of blood vessels with inserted Mg wires, based on the CCA model and material implantation [23], along with the associated blood flow velocity distribution. Post-implantation, the blood flow rate around the Mg wire diminished, yet the blood vessels remained open. The fastest flow rate was proximal, followed by the wire surface, with the

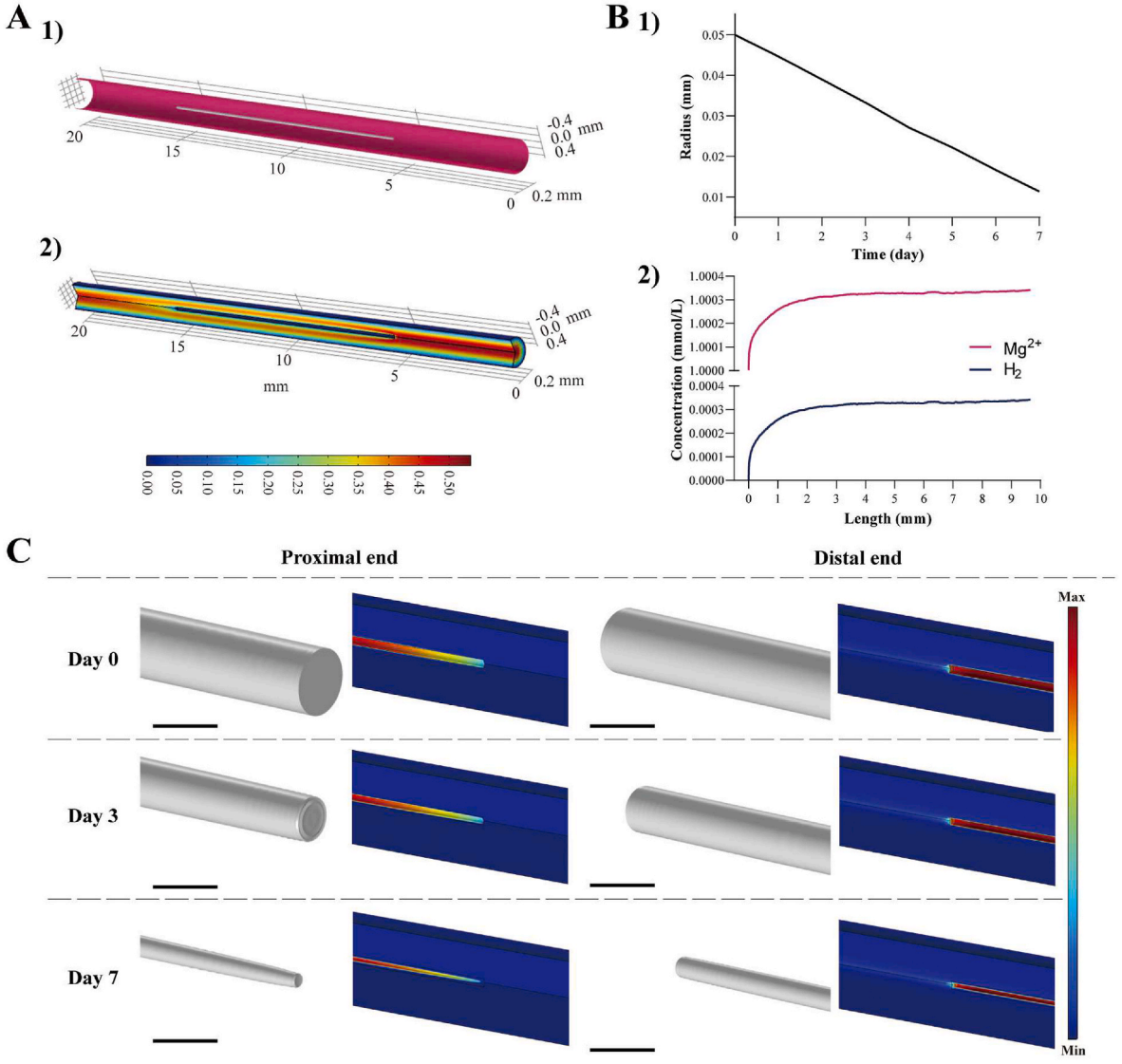

Fig. 2. Computational modeling of Mg wire corrosion within the common carotid artery. (A) The modeling of blood vessels and inserted Mg wires, alongside the corresponding distribution of blood flow velocity within the vessel. (B) The calculated changes in Mg wire diameter over time and the concentration of released Mg^{2+} and H_2 around the wire surface on day 7. (C) The simulated morphological features of the Mg wire over time and the associated contour plots of Mg^{2+} concentration.

distal flow rate being the lowest, all slightly below the central blood flow rate. Fig. 2B revealed changes in the Mg wire's diameter over time. Due to uniform corrosion, the Mg wire diameter linearly decreased with time, exhibiting a corrosion rate of approximately 2 mm/year [24]. Concentrations of magnesium ion and hydrogen released on the wire's surface by day 7 are also presented in Fig. 2B. The high flow rate at the proximal end of the magnesium wire, which induced a higher corrosion rate, led to a rapid initial increase in Mg^{2+} and H_2 concentrations. However, as corrosion rate decreased with increased wire length, the rate of concentration increase gradually slowed, influenced by the diffusion mechanism, which lessened surface concentrations on the Mg wire. Eventually, the concentrations of Mg^{2+} and H_2 on the wire's surface rapidly increased initially and then stabilized.

2.2. In vitro cytotoxicity and neuroprotection analysis

Following computational modeling, the cytotoxicity and neuroprotection of pure Mg degradation were assessed *in vitro*. Cytotoxicity for vascular cells and neurons was evaluated using HUVECs, HASMCs, and HT-22. Initially, cell counting kit (CCK)-8 assays were conducted (Fig. S1, A to C), demonstrating minimal cytotoxicity of various concentration Mg wire extracts on HUVECs, HASMCs, and HT-22 *in vitro*. Concurrently, live/dead cell staining reinforced CCK-8 results (Fig. S1, D and E), showing that compared to control medium, different concentration extracts of pure Mg did not alter live cell ratios. These findings suggest that substances produced during Mg wire degradation do not exert toxic effects on blood vessels and nerve cells.

Subsequently, the *in vitro* neuroprotection of graded Mg^{2+} was evaluated. OGD/R was utilized to mimic I/R injury *in vitro*. Based on CCK-8 and lactic dehydrogenase (LDH) release experiment outcomes, concentrations ranging from 0.4 to 10 mM Mg^{2+} appeared to provide neuroprotection (Fig. S2). Considering substantial neuroprotective capacity of magnesium ion, the impact of Mg extract on neurons was further examined. The Mg extract contained high levels of Mg^{2+} and H_2, exceeding control culture medium amounts (Fig. 3A and B). Additionally, the Mg^{2+} concentration fell within the neuroprotective range (Fig. S2). While both Mg^{2+} and H_2 offered neuroprotection, the potential synergistic neuroprotective effect of Mg extract's Mg^{2+} and H_2 required confirmation. In this study, Mg extract underwent ultrasonic treatment to remove H_2, facilitating a comparison of neuroprotective effects with and without ultrasonication. We measured hydrogen content of the extract after ultrasound and confirmed that the hydrogen was completely removed. The experimental procedure is depicted in Fig. 3C.

First, neuron viability was assessed using the CCK-8 test, while cell death was evaluated through the LDH release test. Post-OGD/R treatment, neuron viability significantly decreased, and cell death increased. These indicators of neuron damage were reduced by 100 % and 50 % Mg extract, but not by 25 % Mg extract. The reversal effect of 100 % Mg extract surpassed that of 50 % Mg extract. Additionally, although 100 % Mg extract post-ultrasonication still exhibited neuroprotection, its efficacy was less than 100 % Mg extract without ultrasonication. Meanwhile, 50 % and 25 % Mg extract after ultrasonication demonstrated no neuroprotection and showed no difference compared to their non-ultrasonicated counterparts, respectively (Fig. 3D and E).

Since H_2 is known as a reactive oxygen species (ROS) scavenger and Mg^{2+} as a natural calcium antagonist inhibiting cellular Ca^{2+} overload, intracellular ROS and Ca^{2+} levels were measured to assess whether Mg wire extract's neuroprotection was due to reduced intracellular ROS production and Ca^{2+} overload. Following OGD/R treatment, both intracellular ROS and Ca^{2+} levels increased. Intriguingly, the effect of different Mg wire extracts on intracellular ROS and calcium mirrored their protective effect on neural cells. 100 % and 50 % Mg extract, and 100 % Mg extract post-ultrasound significantly reduced intracellular ROS and Ca^{2+}. However, 25 % Mg extract and ultrasonically treated 50 % and 25 % Mg extract did not. Moreover, 100 % Mg extract was more effective in inhibiting ROS and Ca^{2+} than 100 % Mg extract post-ultrasound and 50 % Mg extract (Fig. 3F–H).

The results indicate that Mg extract provides dose-dependent neuroprotection, with its neuroprotective effect stemming from the synergistic inhibitory impact of Mg^{2+} and H_2 on ROS production and Ca^{2+} overload.

2.3. In vivo neuroprotection of Mg wires

Given the outstanding *in vitro* neuroprotection by Mg degradation products, Mg wires were implanted in rat CCAs post-ischemia and at the onset of reperfusion to evaluate their neuroprotective effect on reperfusion injury *in vivo*. Concurrently, Ni-Ti wires, commonly used in stent fabrication, were also implanted as a control for the impact of foreign material on blood flow, with their neural effects compared to those of Mg wires. The microstructural characterization and mechanical properties of pure Mg wires were analyzed and presented in Fig. S3. One day post-surgery, compared to the sham group, the MCAO group exhibited severe neurological deficits, with no improvement in the MCAO + Ni-Ti group. However, significant neuroprotection was observed in the MCAO + Mg group (Fig. 4A–C). Notably, the MCAO + Mg group had a lower Longa score, indicating reduced brain motor area damage (Fig. 4A). The elevated body swing test (EBST) score, assessing asymmetry in body movement, was also lower in the MCAO + Mg group compared to the MCAO and MCAO + Ni-Ti groups (Fig. 4B). Furthermore, the rotarod test showed improved locomotor ability recovery post-MCAO in rats with Mg wire implants, evidenced by increased fall latency (Fig. 4C). Although no difference was noted one day post-surgery, the adhesive removal test revealed significantly better sensorimotor function in the MCAO + Mg group compared to the MCAO and MCAO + Ni-Ti groups three days post-surgery, as reflected by decreased removal time (Fig. 4D). The neuroprotective effect of Mg wire implantation persisted for 14 days (Fig. 4A–D).

Seven days post-surgery, an open field experiment was conducted (Fig. 4E). The total movement distance and duration in the MCAO + Mg group exceeded those in the MCAO and MCAO + Ni-Ti groups, indicating greater spontaneous movement engagement in the MCAO + Mg group (Fig. 4F). Additionally, rats in the MCAO + Mg group traversed more and spent more time in the internal peripheral and central areas, suggesting reduced post-infarction anxiety in these rats (Fig. 4F). Therefore, behavioral test results indicated that Mg wire implantation could preserve damaged neurological functions.

2.4. In vivo brain integrity effect of Mg wire

Given the positive neuroprotective effects of Mg wires *in vivo*, rat brains were extracted 7 days post-surgery for *ex vivo* histological examinations. Initially, infarction volume was evaluated using triphenyltetrazolium chloride (TTC) stain. Compared to the sham group, the MCAO group exhibited significant infarction, while the MCAO + Ni-Ti group showed no effect on the infarction area. However, Mg wire implantation demonstrated an inhibitory effect (Fig. 5A and B). Next, Nissl stain, which highlights the Nissl bodies in neurons, was utilized to assess neurocyte integrity. Nissl stain results indicated that in both the cortex and striatum, neuron integrity in the MCAO + Mg group was superior to that in the MCAO and MCAO + Ni-Ti groups (Fig. 5C and D).

BBB disruption is another common consequence of ischemic stroke, potentially worsening prognosis. BBB damage allows water and other harmful macromolecules to infiltrate brain tissue. Therefore, brain water content and brain albumin concentration were measured to gauge BBB leakage. As depicted in Fig. 5E, the MCAO + Mg group exhibited lower water content in the infarcted hemisphere compared to the MCAO and MCAO + Ni-Ti groups. Evans blue staining, which colors albumin passing through the BBB blue, showed that albumin leakage in the MCAO + Mg group was less than in the MCAO and MCAO + Ni-Ti groups (Fig. 5F and G). These histological findings of the brain suggest that Mg wires can effectively preserve brain integrity following ischemic/

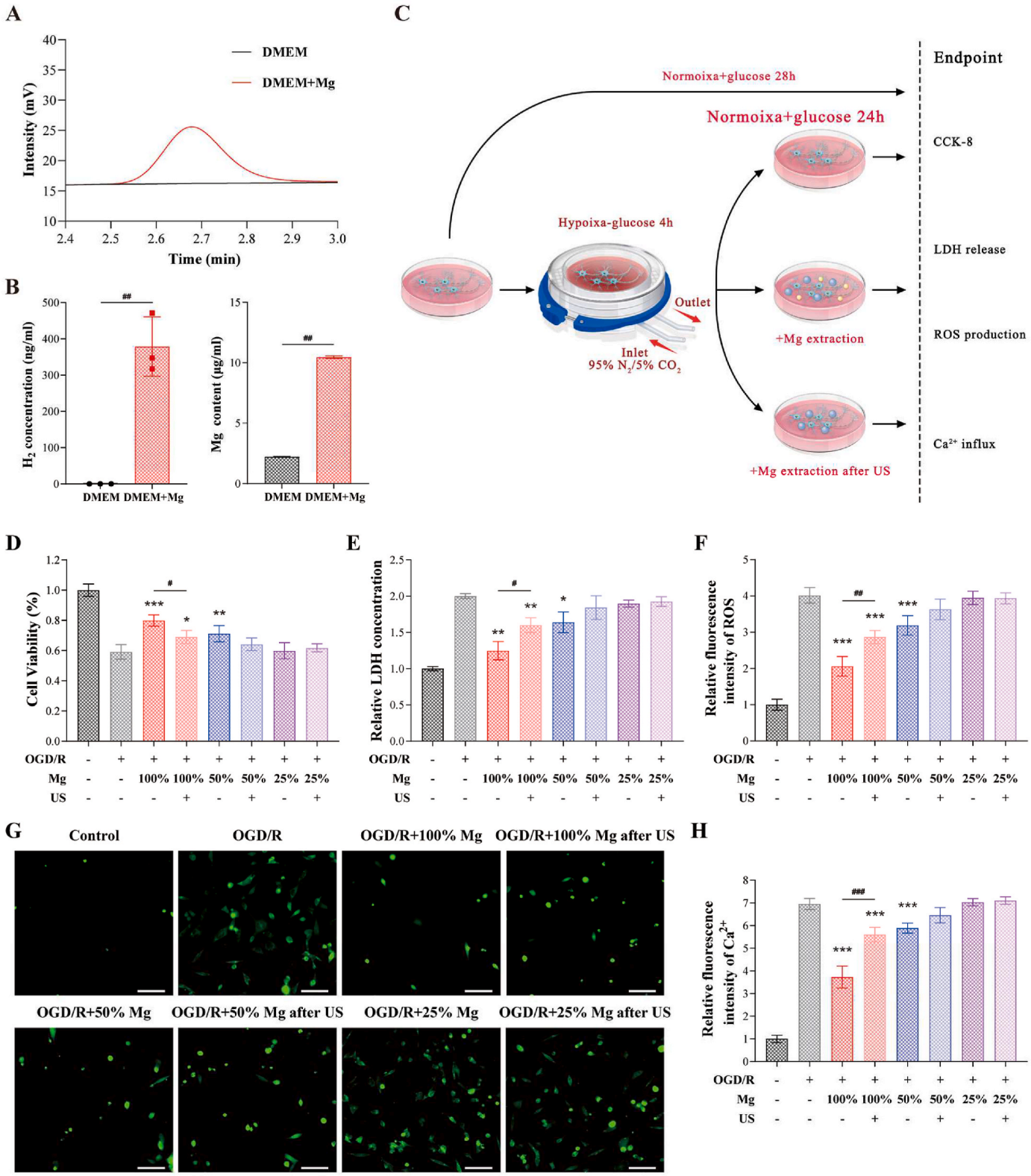

Fig. 3. *In vitro* neuroprotection of Mg wires extract on oxygen-glucose deprivation/reoxygenation (OGD/R) injured cells. (A) Raw data for detecting H_2 through gas chromatography. (B) Quantification of H_2 and Mg^{2+} in normal Dulbecco's Modified Eagle Medium (DMEM) and magnesium wire immersed DMEM. (C) OGD/R cell experimental flowchart. The neuroprotective effect of Mg wires, with or without ultrasound (US) treatment, was evaluated by (D) cell viability, (E) relative lactic dehydrogenase (LDH) release concentration in the supernatant, (F) intracellular relative fluorescence intensity of reactive oxygen species (ROS) in cells and (G) fluorescent images of intracellular Ca^{2+} using a fluorescent microscope, scale bars: 20 μm. (H) Quantification of the fluorescence intensity of Ca^{2+} calculated from (G). Statistical significance is indicated by * $p < 0.05$, ** $p < 0.01$, *** $p < 0.001$ vs. OGD/R group; # $p < 0.05$, ## $p < 0.01$, ### $p < 0.001$.

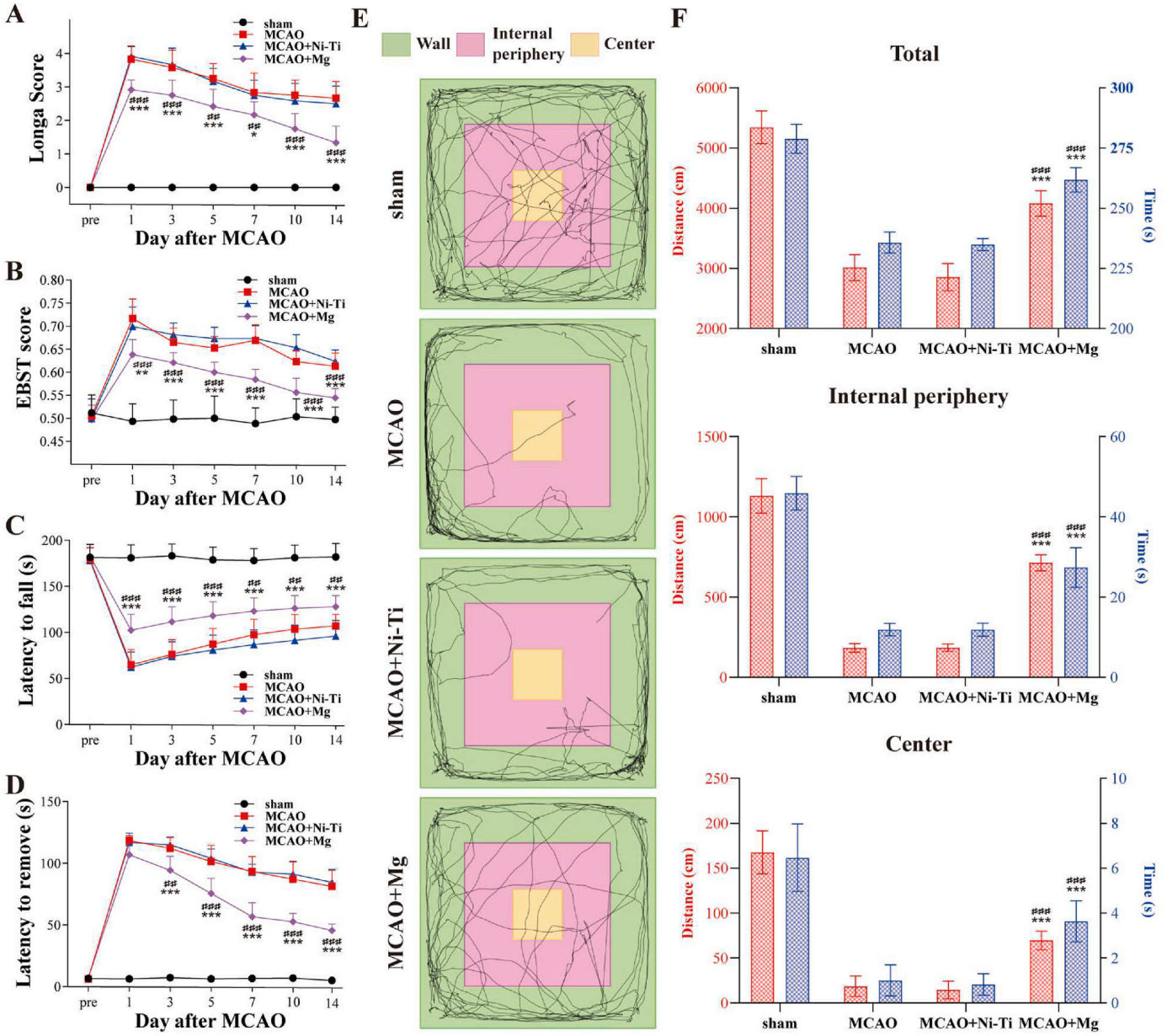

Fig. 4. *In vivo* neuroprotection of Mg wires after ischemic injury. (A) Longa score, (B) elevated body swing test (EBST), (C) rotarod test, and (D) adhesive removal Test were administered before the operation and at 1, 3, 5, 7, 10, and 14 days post-operation. (E) The open field test was conducted 7 days after the operation. (F) The walking distance and time in the open field. The sample size for each group was n = 6 for the sham group and n = 12 for the Middle Cerebral Artery Occlusion (MCAO), MCAO + Ni-Ti, and MCAO + Mg groups. Statistical significance is denoted by * $p < 0.05$, ** $p < 0.01$, *** $p < 0.001$ for MCAO + Mg vs. MCAO group; ## $p < 0.01$, ### $p < 0.001$ for MCAO + Mg vs. MCAO + Ni-Ti group.

reperfusion injury.

2.5. *In vivo* cerebral blood flow effect of Mg wire

Prior studies have shown that both Mg^{2+} and H_2 can dilate vessels post-ischemic/reperfusion injury [6,25]. Consequently, cerebral blood flow (CBF) was monitored before, during, and at 1 and 7 days post-operation. Initially, baseline CBF was consistent across the MCAO, MCAO + Ni-Ti, and MCAO + Mg groups. Upon initiating the MCAO model, CBF on the injured side dropped to about 40 % of the contralateral CBF and recovered to roughly 65 % after 30 min of reperfusion (Fig. 5H and I). Sham surgical procedures and metal wire implantation did not impact CBF (Figs. S4 and S5). On the first day post-reperfusion, CBF in the MCAO and MCAO + Ni-Ti groups remained at approximately 66 %, whereas in the MCAO + Mg group, CBF significantly increased to 81.0 %. Additionally, 7 days post-reperfusion, CBF in Mg wire-treated rats recovered to 95.8 %, markedly higher than in the MCAO and MCAO + Ni-Ti groups (Fig. 5H and I). These CBF results suggest that Mg wire implantation may dilate cerebral vessels, thereby enhancing CBF after ischemic/reperfusion injury.

2.6. *In vivo* corrosion evaluation for Mg wires

The Mg wires implanted in rats were carefully extracted for detailed analysis. Fig. 6A reveals the 3D reconstruction of the remaining Mg wires in the CCA. One day post-implantation, a distinct oxide layer (red) formed on the wire's surface, which was uniform and devoid of tiny corrosion pits. Over time, the oxide layer's thickness increased, and a few pits appeared on the Mg wire matrix, indicating a shift from uniform to localized corrosion with time, possibly due to the oxide layer's

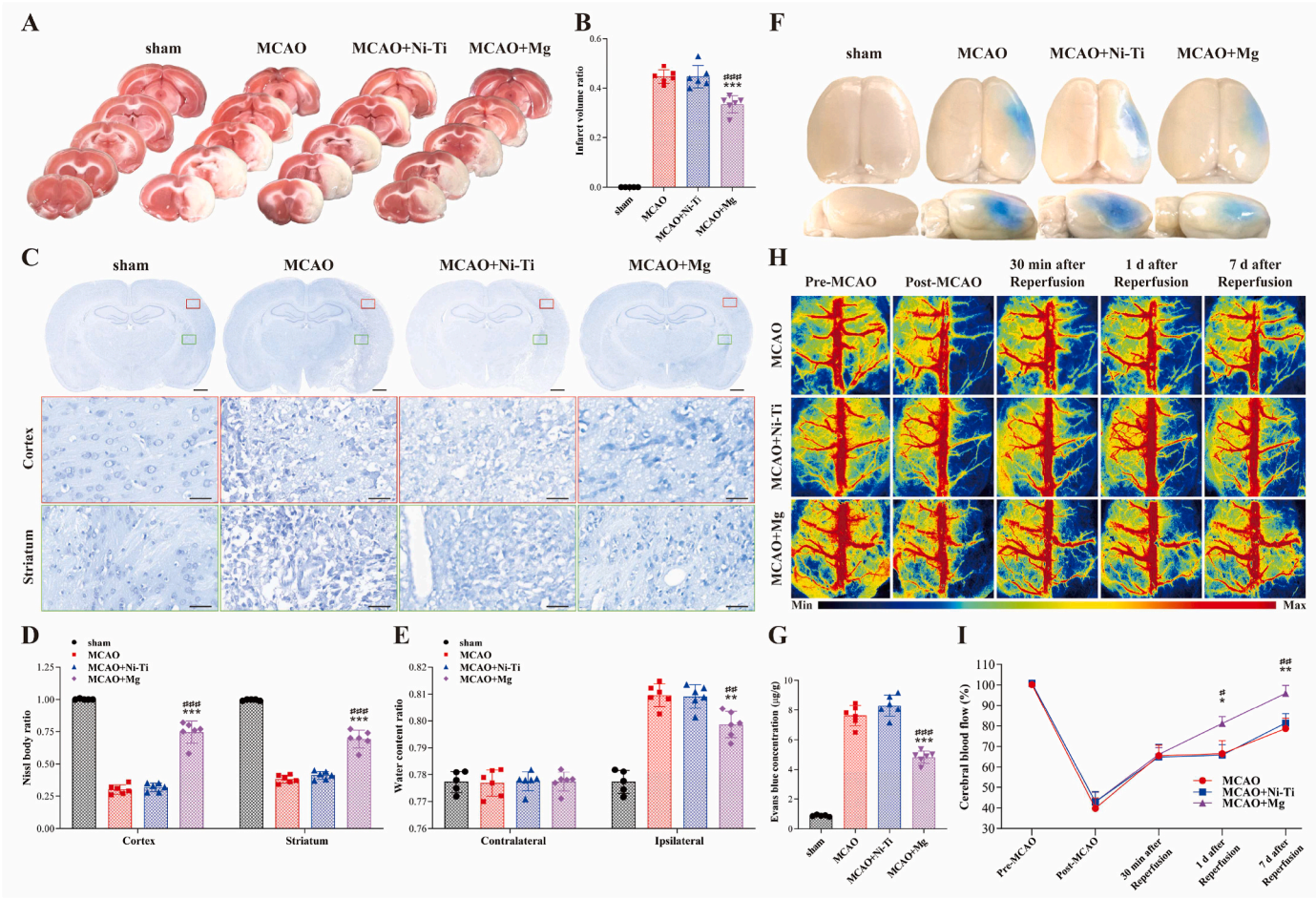

Fig. 5. *In vivo* brain integrity and cerebral blood flow (CBF) preservation of Mg wires on the 7 days after ischemia/reperfusion injury. (A) TTC stain images of brain slices and (B) semiquantitative analysis of infarction volume. (C) Nissl stain images of brain slices and (D) semiquantitative analysis of Nissl bodies; scale bars: 1 mm and 25 μm. (E) Water content ratio of the contralateral and ipsilateral sides of the ischemic brain. (F) Representative images of Evans blue dye extravasation into the brain and (G) quantification of Evans blue content in brain tissue on the infarcted side. (H) CBF images in rats measured by laser speckle imaging at indicated time points. (I) Temporal CBF profile in rats, derived from (H), with the damaged side CBF expressed as a ratio to the contralateral side. Sample sizes were n = 5 for the sham group and n = 6 for the Middle Cerebral Artery Occlusion (MCAO), MCAO + Ni-Ti, and MCAO + Mg groups. Statistical significance is denoted by * $p < 0.05$, ** $p < 0.01$, *** $p < 0.001$ for MCAO + Mg vs. MCAO group; # $p < 0.05$, ## $p < 0.01$, ### $p < 0.001$ for MCAO + Mg vs. MCAO + Ni-Ti group.

degradation. The residual volume of Mg wire gradually decreased with time, from 80.55 ± 1.65 % on the first day to 66.64 ± 0.91 % on the 28th day (Fig. 6B), suggesting a decreasing corrosion rate in rats. Nevertheless, the Mg wires maintained structural integrity a month after implantation. Fig. 6B and C, display the residual volume during Mg wire corrosion and the release of hydrogen and magnesium ions into the physiological environment. The release rate of hydrogen and magnesium corresponded with Mg wire corrosion, gradually decreasing over time. Besides the magnesium released into the physiological environment, magnesium also remained in the corrosion layer. Hence, the amount of magnesium ions released (red line in Fig. 6C) is estimated based on the magnesium content in the corrosion layer (Fig. 6A). The estimations indicate that on the first day post-implantation, approximately 1.00 ± 0.085 μmol of magnesium and 1.11 ± 0.094 μmol of hydrogen gas were released into the blood. Over one month of implantation, about 1.7 μmol of magnesium and 1.9 μmol of hydrogen were released, highlighting that the release was concentrated in the early stages of implantation. Fig. 5D displays the surface morphologies of the Mg wires and corresponding energy-disperse spectrometer (EDS) element mapping, revealing a thin degradation product layer composed of Ca, P, O, and Mg on the Mg wires. The Mg content in this layer was found to decrease with increased corrosion time (Fig. 6E), aligning with prior research [21]. In general, Mg wires in the CCA exhibited uniform corrosion *in vivo*, with the fastest corrosion rate observed on the first day, which gradually diminished over the duration of implantation.

2.7. *In vivo* Mg^{2+}, H_2, ROS and Ca^{2+} concentration and biosafety tests

The Mg^{2+} concentration in blood and various organs, including the heart, liver, spleen, lung, kidney, infarction contralateral brain (ICB), and infarction ipsilateral brain (IIB), was measured in different rat groups at 1 and 7 days post-operation. On day 1 post-operation, the Mg^{2+} concentration in the MCAO + Mg group's blood was higher than in the sham, MCAO, and MCAO + Ni-Ti groups, and this concentration decreased by day 7 (Fig. 7A). The concentration of Mg^{2+} in rat carotid blood and infarction brain was measured to have increased by about 18 μg/g, which is on the same order of magnitude as *in vitro*. Except for the IIB on day 1, Mg^{2+} levels in all tested organs showed no significant differences (Fig. 7B, and Fig. S6). The concentration of Mg^{2+} in rat CCA blood and infarction brain was measured to have increased by about 18 μg/g, which is on the same order of magnitude as *in vitro*. Additionally, a small but detectable amount of H_2 was found in the blood on day 1 post-operation (Fig. 7C and D). Hydrogen gas in the brain was also measured after take out the brain from rats, but H_2 was not detected. In the future, Hydrogen-1 magnetic resonance spectroscopy may be used for detection at the *in vivo* level [26].

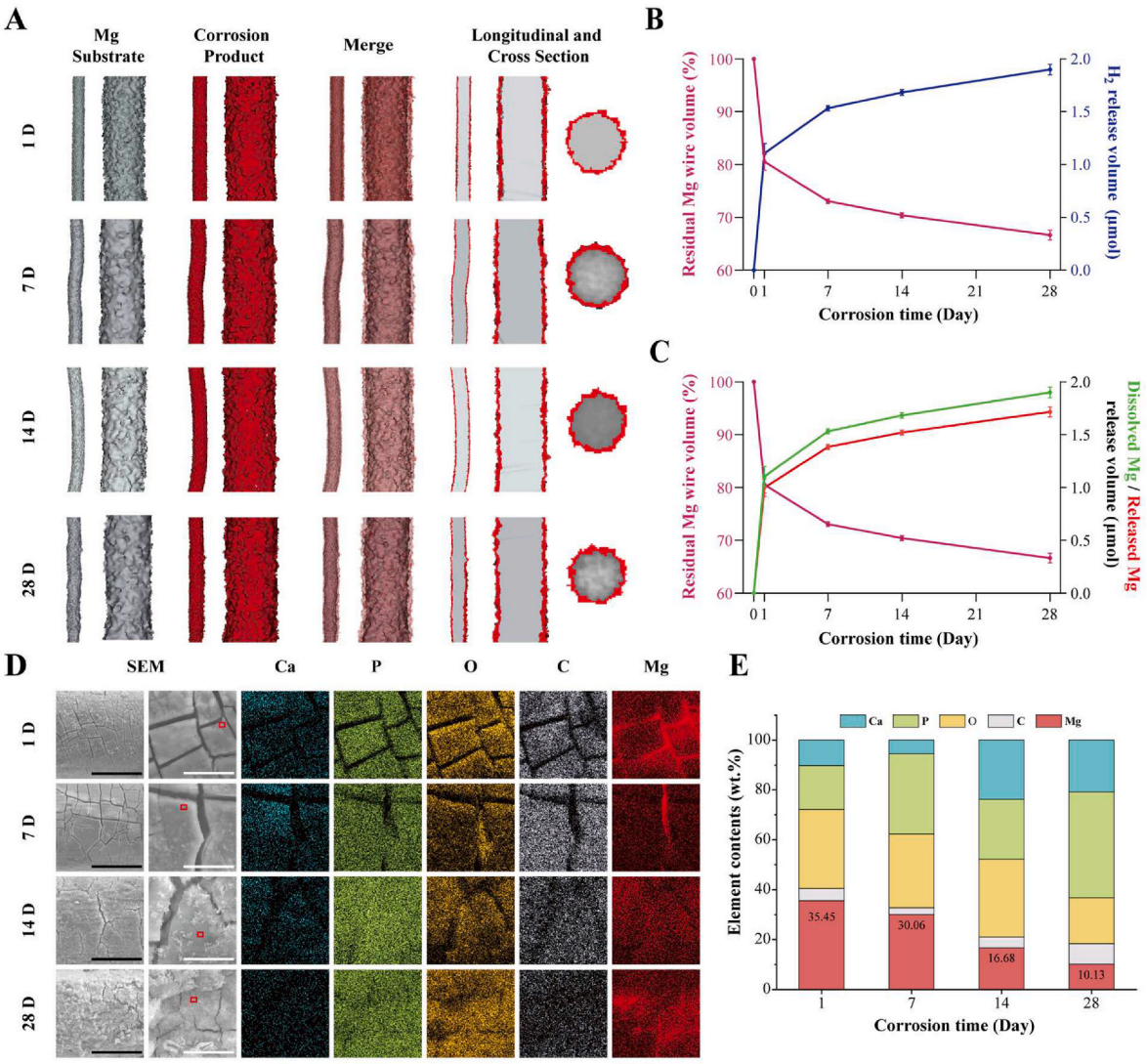

Fig. 6. *In vivo* corrosion evaluation for Mg wires. (A) 3D reconstructions of the residual Mg wires and corrosion products at 1, 7, 14, and 28 days post-implantation, based on micro-computed tomography analysis. (B) The residual Mg wire volume and the volume of released hydrogen over time. The residual Mg wire volume is derived from simulation results, while the volume of released hydrogen is calculated based on this residual volume. (C) The residual Mg wire volume and the magnesium dissolved/released into the physiological environment over the course of implantation. (D) Scanning electron microscope images and energy-disperse spectrometer (EDS) element mapping of the Mg wires after 1, 7, 14, and 28 days of implantation. The black and white scale bars represent 50 and 10 μm, respectively. (E) The EDS point analysis results of the degradation products on the Mg wires' surface.

From these results, it is inferred that the implantation of Mg wires led to the release of Mg^{2+} and H_2 into the blood during Mg wire degradation, most notably on the first day. Although this release slowed over time, substantial Mg^{2+} and H_2 were still present in the blood on day 7. Regarding brain tissue in the damaged area, the severe BBB disruption on day 1 allowed a large influx of blood-borne Mg^{2+} into the brain parenchyma. By day 7, some BBB recovery had occurred, reducing the influx of Mg^{2+} into the IIB, thus reaching a balance with Mg^{2+} elimination. Since BBB does not impede hydrogen, the hydrogen levels in the IIB were likely proportional to those in the blood (Fig. 7E).

In addition to Mg^{2+} and H_2, concentrations of cerebral ROS and Ca^{2+} were also measured. Mirroring the *in vitro* findings, ROS and Ca^{2+} levels in the ICB did not differ among the four groups. However, in the IIB, ROS and Ca^{2+} levels were elevated in the MCAO and MCAO + Ni-Ti groups, while Mg wire implantation significantly inhibited this increase (Fig. 7F and G). Furthermore, rats were euthanized after 1, 7, 14, and 28 days of Mg wire implantation for histological analysis. The main organs were excised and stained with H&E, which showed no apparent acute or chronic pathological toxicity, nor adverse effects in either control or treatment groups (Fig. S7). Moreover, Mg content in the brain had returned to the normal range by the seventh day after implantation, which may be due to BBB recovery and rapid metabolism of Mg^{2+}, and in our observation, the rats still maintained a state of neurological function recovery at 14 days after operation, so we speculated that the temporary increase in Mg^{2+}in the brain was unlikely to have long-term adverse effects on neurological function.

3. Discussion

This study explored the neuroprotective effects of Mg implants using OGD/R-induced HT-22 cells and MCAO rat models to simulate human brain ischemia. Pure Mg extract was found to play a protective role in aiding HT-22 cells in defending against OGD/R injury. Additionally, a pure Mg wire was implanted into the CCA of MCAO rats, analogous to inserting a biodegradable neuroprotective Mg stent into cerebral vessels. Observations revealed that pure Mg wire implantation facilitated various benefits, including neurorescue, BBB protection, and CBF improvement (Fig. 8). Based on the findings of this study, the innovative

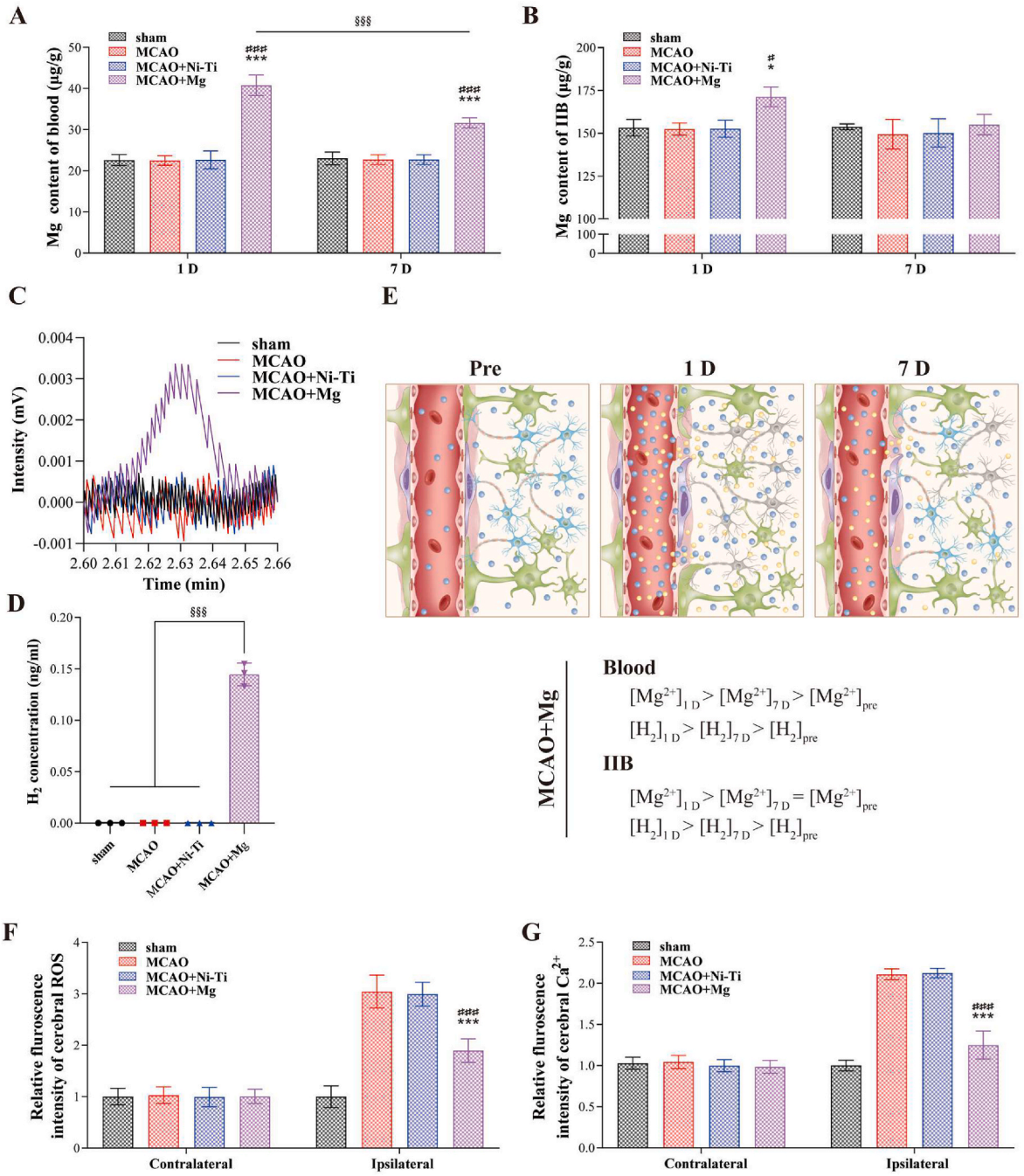

Fig. 7. *In vivo* Mg^{2+}, H_2, reactive oxygen species (ROS) and Ca^{2+} concentration in blood and brain. The concentration of Mg in the (A) blood and (B) infarction ipsilateral brain (IIB) of rats at 1 and 7 days post-implantation of Mg wires (n = 3). (C) Raw data and (D) quantification of H_2 in rat blood tested by gas chromatography. (E) The map and inference of the distribution of Mg^{2+} and H_2 in blood and brain tissue. The relative fluorescence intensity of cerebral (F) ROS and (G) Ca^{2+} is also depicted. The sample size for each group was n = 5 for the sham group and n = 6 for the Middle Cerebral Artery Occlusion (MCAO), MCAO + Ni-Ti, and MCAO + Mg groups. Statistical significance is indicated by $^{**}p < 0.01$, $^{***}p < 0.001$ for MCAO + Mg vs. MCAO group; $\#\#p < 0.01$, $\#\#\#p < 0.001$ for MCAO + Mg vs. MCAO + Ni-Ti group.

concept of "biodegradable neuroprotective stents" appears promising and warrants further investigation in future research endeavors.

3.1. Mg alloy in neuroscience

Mg and its alloys are gaining recognition as promising alternatives to permanent biomedical materials, thanks to their adjustable mechanical strength and biodegradability [27,28]. However, the use of Mg-based biomedical devices in neuroscience is still in its early stages [29–31]. Potential applications include nerve guidance conduits [27,32], major components of nerve electrodes for neural recording or monitoring [33,34], cerebral aneurysm coil-assisted stents [35], and common carotid artery stents [36].

The biodegradable Mg alloy cardiovascular stent named Magmaris (DREAMS 2G), achieved its CE mark in 2016, demonstrating clinical safety and efficacy [37]. The cerebrovascular system, characterized by its tortuosity and lack of perivascular tissue support, is more susceptible to rupture under hemodynamic stress compared to cardiovascular vessels. The hydrodynamic characteristics of the stent's deployment site also significantly influence Mg alloy degradation behaviors [38].

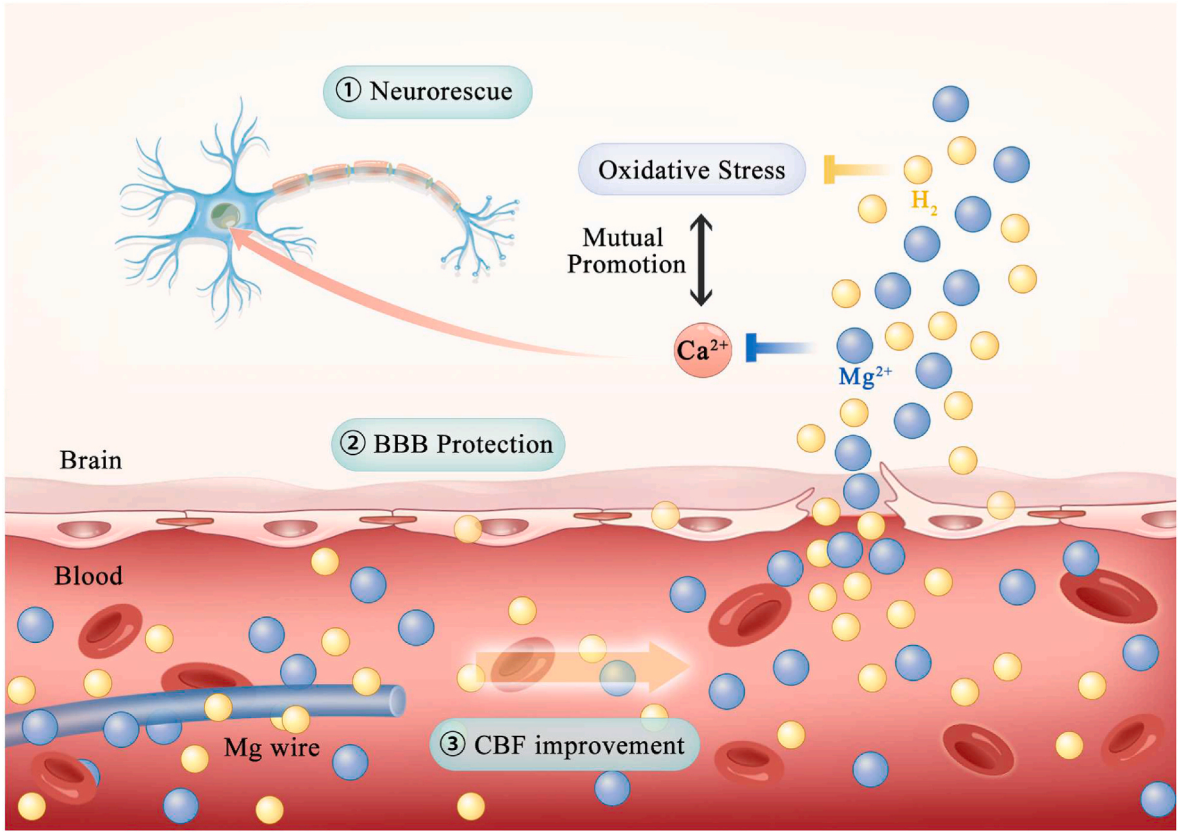

Fig. 8. Illustration of the effect of Mg wire in the ischemic brain. The Mg^{2+} and hydrogen generated by the degradation of Mg wires travel to the damaged site and cross the BBB into the brain. Mg^{2+} and hydrogen primarily inhibit the influx of Ca^{2+} and the production of ROS, respectively, and exhibit a synergistic relationship, ultimately leading to neuron rescue, BBB protection, and enhanced CBF.

Varying wall shear stresses are observed in different blood vessels in the human body, such as 0.68 ± 0.03 Pa in the coronary artery, 1.23 ± 0.21 Pa in the carotid artery, and 1.62–2.29 Pa in the cerebral artery [39,40]. Therefore, ensuring the mechanical compatibility and uniform corrosion of Mg alloy stents is crucial for their potential application in cerebral scenarios. Moreover, our research is to investigate the neuroprotective effects of degradation products of Mg metal materials, providing theoretical support for the development of neuroprotective Mg alloy stent and also providing new ideas for Mg based neural implant devices (degradable nerve electrodes, coils). The corrosion rate of Mg alloys is related to their surface area and local fluid environment [41]. Thus, it is necessary to recalculate the Mg release concentration of Mg alloy stents, nerve electrodes, and coils based on specific circumstances.

3.2. Intracranial stenting and reperfusion injury

Intracranial atherosclerotic stenosis is a leading cause of stroke worldwide. The SAMMPRIS and VISSIT randomized controlled trials (RCTs) showed that intracranial stenting was less effective than drug therapy, primarily due to high complication rates associated with stenting [42]. Furthermore, combining stenting with medical therapy did not significantly reduce stroke or death risks in patients with symptomatic intracranial stenosis compared to medical therapy alone [43].

A potential explanation for these suboptimal stenting outcomes could be related to cerebral ischemia-reperfusion injury or cerebral hyperperfusion syndrome [44]. Recanalizing occluded vessels and restoring blood supply in ischemic strokes often triggers various molecular and cellular responses. Among these, Ca^{2+} overload and ROS production are key factors in reperfusion neural injury development. The BBB comprising endothelial cells, basement membrane, pericytes, and astrocyte end feet, plays a vital role in maintaining cerebral homeostasis. Intracellular Ca^{2+} and ROS in endothelial cells are critical mediators that affect BBB permeability [45]. Disruption of the BBB increases vascular permeability, leading to further brain damage [46]. Thus, neuroprotective strategies are crucial for addressing ischemic brain injury post-recanalization. Although over 1000 potential neuroprotectants have shown promise in preclinical studies, they often fail in clinical trials [47], underscoring the need for novel treatments.

3.3. Neuroprotection of Mg^{2+} and H_2

Magnesium ion supplementation offers various neuroprotective mechanisms in cerebral ischemic diseases [6]. Mg^{2+} reduces intracellular calcium overload mediated by the N-methyl-d-aspartate receptor and acts as a natural calcium antagonist. It also dilates cerebral vessels, enhancing blood flow post-cerebral ischemia, stabilizes mitochondrial function and regulates enzymes critical for energy metabolism in the brain post-ischemia. Mg^{2+} can be administered intraperitoneally, intravenously, arterially, and intracranially. Carotid artery injection, in particular, can rapidly increase drug concentration at the target site with a lower dose [48].

Additionally, molecular hydrogen has emerged as a therapeutic medical gas effective in treating various brain diseases by eliminating cytotoxic oxygen radicals. This was first demonstrated in 2007, where inhaling hydrogen was shown to attenuate brain injury by reducing neural ROS damage in an I/R injury rat model [9]. Similar neuroprotective effects of hydrogen were observed in a global cerebral I/R mouse model [49] and in OGD/R-damaged hippocampal neurons, where hydrogen was found to promote mitophagy via the PINK1/Parkin signaling pathway, preserving mitochondrial membrane potential [50]. Hydrogen administration methods include non-invasive approaches like

inhalation of hydrogen gas and drinking hydrogen-rich water, which are portable, safe, and simple, but deliver limited doses to the target area. In contrast, invasive methods like hydrogen dissolved saline injections into the peritoneum or blood vessels can deliver enough hydrogen to the injured area [11].

According to these findings, beyond the individual effects of magnesium and hydrogen, their combined use may offer enhanced neuroprotection. A recent clinical trial demonstrated that intracisternal $MgSO_4$ infusion coupled with intravenous hydrogen therapy improved patient rehabilitation following severe aneurysmal subarachnoid hemorrhage more effectively than either $MgSO_4$ infusion alone or control treatments [18]. These results suggest that combination therapy using Mg^{2+} and hydrogen could be more effective in treating ischemic stroke synergistically compared to monotherapy. This hypothesis aligns with the *in vitro* experiment in the current study. Additionally, while H_2 primarily protects against ROS overproduction, its deprivation from Mg wire extract also reduced its inhibitory effect on Ca^{2+} overload. This could be due to the complex interplay between ROS and Ca^{2+} signaling, where abnormalities in one can affect the other, destabilizing both pathways. Conversely, protecting one pathway might safeguard the other, thus stabilizing both [51].

Besides its direct neuroprotective impact, this study's *in vivo* research also found that Mg wire implantation protected the BBB and promoted CBF recovery post-cerebral infarction. Ca^{2+} overload and ROS are known factors in EC damage, leading to increased BBB leakage [46]. Concerning CBF, Ca^{2+} overload and ROS are principal causes of pericyte contraction, reducing vascular diameter and CBF [52,53]. It is speculated that these effects are achieved through the synergistic inhibition of Mg^{2+} and H_2 on Ca^{2+} overload and ROS in ECs and pericytes. However, further research is necessary to confirm this hypothesis.

It is worth noting that we could not separate Mg^{2}+ and H_2 *in vivo*, and currently it is also difficult to fully simulate the process of degradation of Mg wires *in vivo* through continuous injection of Mg^{2+} or H_2. If the filtration of Mg^{2+} or H_2 in blood *in vivo* can be achieved in the future, we will further explore their respective roles. Meanwhile, at present, we could not determine which is more important, Mg^{2+} or H_2, as their protective effects are regulated by multiple factors *in vivo*, such as concentration [7,9], injection method [54,55], intervention timing [6,12]. If we can determine in the future, coating Mg wires/stents with polymer loaded with soluble Mg salt to release more Mg^{2+} or alloying to release more H_2 [56,57] to improve the implanted Mg wires/stents seems to be a promising direction.

3.4. Neuroactivity of pure Mg metal and Mg alloys

Direct studies on the neuroactivity of pure Mg metal or Mg alloys are relatively scarce, but the neuroprotective properties of Mg ions, typically in the form of $MgSO_4$ or $MgCl_2$ solutions, have been extensively researched. Our previous work revealed that Mg^{2+}, sourced from a pin containing ultrapure magnesium implanted in the intact distal femur of rats, promoted new bone formation and significantly increased neuronal calcitonin gene-related peptide (CGRP) in the ipsilateral dorsal root ganglia (DRG) and the peripheral cortex of the femur [58]. Further, isolated rat DRG neuron experiments indicated that elevated extracellular Mg^{2+} could trigger Mg^{2+} influx through specific channels, enhance intracellular adenosine triphosphate (ATP) levels, and accumulate terminal synaptic vesicles containing CGRP. This might boost osteogenic differentiation of periosteum-derived stem cells, suggesting that Mg^{2+} from pure Mg metal could enhance neural energy metabolism.

Additionally, research found that diluted extracts of Mg-Zn-Nd-Zr magnesium alloy stimulated the proliferation of astrocytes and neural stem cells [59]. This extract also encouraged differentiation from neural stem cells into astrocytes and neurons [59]. These effects might largely be due to Mg^{2+} in the extract, as Mg^{2+} is known to promote the proliferation and differentiation of neural stem cells [60,61].

In conclusion, while research on the neuroprotective effects of pure Mg metal and Mg alloys is limited, the existing studies provide valuable insights. The protective effect of pure Mg wire on nerves following AIS might also be attributed to the improvement of energy metabolism in nerve cells and the facilitation of neuronal regeneration.

Moreover, neurotoxicity aspect also deserves attention. According to *in vivo* animal study, the complete degradation of Mg wire in the CCA of rats takes about 3–4 months [62,63]. During this period, we did not observe the related adverse reactions such as small vessel occlusion or neural activity and behavior change. The speculated reason is that the Mg^{2+} and H_2 produced by the degradation of Mg wire can be safely metabolized in the body.

3.5. In vivo activity of H_2 from the metal source

The *in vivo* effects of H_2 derived from metal implants have been a focus of recent research. For instance, Yang et al. developed Mg-based galvanic cells (MgG) for implantation into tumors. Their study found that MgG could produce H_2, inducing mitochondrial dysfunction and disrupting intracellular redox homeostasis in tumors, thereby inhibiting tumor growth [64]. Similarly, Liu et al. leveraged the anti-inflammatory properties of H_2 by constructing a Zn-Fe battery. This battery, when orally delivered to the stomachs of diabetic model mice, enhanced Zn hydrolysis, producing H_2 which then reduced systemic inflammation [65]. In another study, Nan et al. incorporated Mg particles into microparticles for injection into the knee joint. The H_2 generated during Mg degradation was found to inhibit ROS production, thereby reducing joint inflammation [66]. These studies demonstrate the versatile *in vivo* activities of H_2 from Mg sources, with our research further extending this field into neuroprotection. Moreover, the safety of producing hydrogen gas in the blood is worth exploring, as gas can form gas clots in the blood. However, due to the flowing state of the blood around the Mg wire, the hydrogen gas produced by the Mg wire will continuously flow with the blood flow and will not accumulate locally. Moreover, our study did not find any adverse consequences similar to gas embolism, which is sufficient to prove the vessel safety of the Mg wires.

3.6. Stent with "remote" neuroprotection

The concept of "remote" is well-established in medicine. For example, remote ischemic lesion refers to ischemic injuries occurring distally from an intracranial hemorrhage site, potentially due to vasospasm caused by a hematoma [67]. The remote bioactivity of materials or techniques is also being explored. Peng et al. discovered that local implantation of polypropylene and silk fibroin in the abdomen could lead to remote liver fatty deposition [68]. Remote ischemic conditioning, involving repeated transient ischemia of the limbs using blood pressure cuffs, has been shown to protect distant organs like the heart or brain from further ischemic damage [69]. This technique has been validated in multi-center RCTs [70,71]. Drawing on these principles, our research proposes the concept of a "biodegradable remote neuroprotective stent." This concept is based on the finding that locally released Mg^{2+}/H_2 from Mg metal within blood flow can offer synergistic neuroprotection to distant cerebral ischemic tissues. Future stent designs could benefit from this innovative approach to endow the stent with neuroprotective function.

There are many branches of arteries in the rats and this phenomenon is consistent with the human environment. However, we did find an increase in Mg^{2+} concentration in the infarction brain of rats (Fig. 7B), which is sufficient to prove the targeted therapeutic potential of stent with neuroprotective materials.

3.7. Future development

The current study lays the groundwork for future research in the development of biodegradable Mg alloy stents, particularly for neurovascular applications. Several key areas are suggested for further

exploration.

1) In this research, pure Mg wires were utilized to isolate the neuroprotective effects from other metal elements. However, pure Mg's inadequate mechanical properties and uncontrolled corrosion rate make it unsuitable for stent fabrication [72]. These issues can be addressed through alloying and surface modification. The alloying process, which involves adding other metal elements, opens the possibility of investigating the neuroprotective effects of these additional elements. Moreover, surface modifications, typically through coatings, present opportunities to incorporate drugs like edaravone [73] or butylphthalide [74], which have been shown to aid in cerebral infarction recovery.
2) Stroke treatment is time-sensitive, making it crucial to align the degradation rate of Mg alloys with the treatment window. This alignment could be achieved through surface engineering techniques, such as plasma immersion ion implantation and deposition (PIIID) technology, which could create stents with tailored corrosion rates for specific timeframes [37].
3) Currently, magnesium alloy biodegradable stents are only approved for coronary diseases. Given the common pathogenic factors shared by cardiovascular and cerebrovascular diseases [75], it is crucial to investigate the potential protective effects of coronary magnesium alloy stents on cerebrovascular diseases during their degradation.
4) Besides cerebral infarction, strokes also include subarachnoid hemorrhage, often resulting from aneurysm rupture [76]. Stent-assisted coil embolization is a common treatment for ruptured aneurysms [77]. Thus, Mg alloy stents could potentially be used in treating cerebral aneurysms, and the impact of stent degradation on neural functions post-subarachnoid hemorrhage represents another research avenue.
5) Based on this study, when Mg alloy stents can be applied in the cerebral vessel in the future, clinicians can not only focus on the impact of Mg stents on *in situ* blood vessels compared to traditional stents, but also conduct RCTs to explore whether Mg alloy stents have additional neuroprotective effects, providing direct evidence for the clinical application of neuroprotective stents.

4. Conclusions

In summary, this study investigated the use of Mg metal as an endovascular device in neuroscience. The Mg extract was found to protect mouse hippocampal neuronal cells against OGD/R injury. The locally released Mg^{2+}/H_2 from the Mg wire implanted in the MCAO rat model offered synergistic neuroprotection to remote cerebral ischemic tissues. Mg^{2+} and H_2 primarily inhibited Ca^{2+} influx and ROS production, respectively, with a mutual enhancement of their effects, leading to neuron rescue, BBB protection, and improved cerebral blood flow. These findings introduce an innovative stent design concept: "biodegradable neuroprotective stents".

5. Materials and methods

5.1. Implanted materials

Pure Mg wires with a diameter of 0.10 mm were created using a cold-drawing process from Mg bars of 10.0 mm diameter. These bars were hot extruded at 200 °C with an extrusion ratio of 25:1. All samples used in the experiment underwent ultrasonic cleaning in acetone, absolute ethanol, and distilled water, each for 10 min. The microstructures and morphology of the samples were then analyzed using an X-ray diffractometer (XRD, Rigaku DMAX 2400, Japan) and a scanning electronic microscope (SEM, S-4800, Hitachi, Japan). Tensile strength measurements were conducted using a universal material test machine (Instron 5969, USA) at a displacement rate of 1 mm/min at room temperature.

To evaluate the evolution of magnesium ions and hydrogen gas *in vitro*, Mg wires of ϕ0.1 mm diameter and 10 mm length were immersed in SBF at 37 °C. The solution volume to sample surface area ratio was maintained at 20 ml/cm^2 as per ASTM G31-72 standard. Five parallel samples were used for each group. Post-immersion, magnesium ions concentrations in SBF were measured using Inductively Coupled Plasma Optical Emission Spectroscopy (ICP-OES, iCAP6300, Thermo).

5.2. Computational modelling of in vivo corrosion

The corrosion behavior of the implanted Mg wire within the rat CCA was simulated using COMSOL Multiphysics® software. A 2D axisymmetric simplified method was applied, focusing on mass transfer related to flow-induced corrosion in a constructed rational swept surface. The laminar flow module within Computational Fluid Dynamics was utilized to simulate the relative flow velocity of blood around the Mg wire in the vessel. The velocity field for this simulation was solved using the Navier-Stokes equation:

$$\rho(\boldsymbol{\upsilon}\cdot\nabla)\boldsymbol{\upsilon} = \nabla\cdot[-p\mathrm{I}+\mathrm{K}]+\mathbf{F}+\rho\mathbf{g}$$

$$\nabla(\rho\boldsymbol{\upsilon}) = 0$$

where.

ρ is the density (kg/m^3)
$\boldsymbol{\upsilon}$ is the velocity vector (m/s)
p is the pressure (Pa)
K is the viscous stress tensor
F is the volume force vector

The conservation calculation of convection mass transfer in this study is based on the previously calculated convection velocity. This approach ensures adherence to the requirements of the transport of the diluted species interface module. The mass transfer process is simulated using a diffusion equation:

$$\nabla\cdot(-D\nabla c)+\boldsymbol{\upsilon}\bullet\nabla c = 0$$

where.

c is the concentration (mol/m^3)
D is the diffusion rate (m^2/s)

This model primarily focuses on surface reactions rather than bulk reactions, adhering to Fick's laws of diffusion. Within this equation, the variable υ represents the convective term. Additionally, the surface mass flux of the Mg wire is calculated under the surface electrochemical reaction rate. This calculation is crucial for simulating the boundary movement, which is achieved using the moving grid method. The speed of grid movement on the Mg wire surface is considered indicative of the corrosion rate of Mg, which is calculated using the following equation:

$$v_n = k\,M_{mg}/\rho_{mg}$$

Where.

k is the surface reaction rate (mol/m^2/s)
M_{mg} is the molar mass of Mg (g/mol)
ρ_{mg} is the density of Mg (kg/m^3)

As for physical field boundary settings, the relative inlet boundary of the fluid is 12.23 mL/min, and the Mg inlet concentration is 0.46 mmol/L.

5.3. Cell experiments

5.3.1. In vitro cytotoxicity assays with pure Mg extracts

The cytotoxicity effects of pure Mg on ECs, smooth muscle cells, and neurons were evaluated. Human umbilical vein endothelial cells (HUVECs), human artery smooth muscle cells (HASMCs), and HT-22 (mouse hippocampal neuronal cell line) served as the instrumental cells for these experiments. Pure Mg wires were immersed in DMEM supplemented with 10 % fetal bovine serum and 1 % penicillin/streptomycin to prepare the extracts. Cells were cultured in a humidified atmosphere with 5 % CO_2 at 37 °C. The culture periods were set at 1, 3, and 5 days using either the control medium (DMEM) or Mg extracts at concentrations of 100 %, 50 %, and 25 % (diluted with DMEM). The viability of the cells was evaluated using the CCK-8 assay (Beyotime, China). The spectrophotometric absorbance of each well was measured using a microplate reader (ThermoFisher Scientific, USA) at a wavelength of 450 nm. In addition, after one day of culture, cells were stained using the LIVE/DEAD® assay (Invitrogen, USA), following the manufacturer's instructions. A mixed solution of Calcein-AM and PI was added to each cell well and incubated for 30 min. Subsequently, the solution was removed, and the cells were observed under a fluorescence microscope (EVOS, AMG). Living cells were stained green with Calcein-AM, while dead cells were stained red with PI.

5.3.2. In vitro neuroprotection assessments with pure Mg extracts

To simulate I/R injury *in vitro*, cells were subjected to OGD/R injury [78]. HT22 cells were maintained in a glucose-free culture medium and transferred to a 37 °C anaerobic chamber containing 5 % CO_2 and 95 % N_2 for a 4-h incubation. Subsequently, the medium was replaced with regular DMEM containing glucose, and the cells were returned to a normoxic environment for 24 h of reoxygenation at 5 % CO_2/95 % air. As a control, normal DMEM with glucose was used, incubated under identical conditions. Following the OGD technique, DEME with gradient Mg^{2+} concentrations, both ultrasonically treated and untreated (100 %, 50 %, and 25 %) Mg extracts containing glucose, served as the medium for incubating HT22 cells for 24 h at 37 °C. Post-incubation, cell viability, LDH release, ROS production, and Ca^{2+} influx were evaluated.

Cell viability was first assessed using the CCK-8 kit as previously described. LDH, released from cells when plasma membrane integrity is compromised, indicates the degree of cell death. We measured LDH release using an LDH assay kit (Beyotime, China). The cell supernatants were incubated with the assay kit solution, and the resultant color change was quantified by spectrophotometry at 490 nm. Secondly, ROS, produced during oxidative stress, were detected using DCFH-DA (Beyotime, China). Cells were incubated with 10 μM DCFH-DA in a serum-free medium, washed thrice, and lysed with 50 % methanol containing 0.1 M NaOH. After detaching and centrifuging the cells, the supernatants were collected, and fluorescence at 488/525 nm was measured using a fluorescence microplate reader. Lastly, intracellular Ca^{2+} influx, indicative of oxidative stress damage, was assessed with the Fluo-4 calcium assay kit (Beyotime, China). Cells were incubated with Fluo-AM solution, imaged using a fluorescent microscope, and the fluorescent intensity of Fluo-4 AM was quantified using Image J software.

5.4. Animal experiments

The study involved adult male Sprague-Dawley (SD) rats, each weighing between 280 and 320 g. The Institutional Animal Investigation Committee of Capital Medical University approved all experimental methods, ensuring that all animal treatments adhered strictly to the National Institutes of Health's guidelines for the Care and Use of Laboratory Animals.

5.4.1. MCAO model and material implantation

Rats were grouped as follows: Sham Group (underwent only preoperative anesthesia and vascular separation surgery); MCAO Group (underwent the MCAO procedure without any material implantation); MCAO + Ni-Ti Group (underwent MCAO with Ni-Ti wire implantation); MCAO + Mg Group (underwent MCAO with Mg wire implantation). Rats received aspirin (10 mg/kg/day) and clopidogrel (7.5 mg/kg/day) regimens starting three days before the procedure and continuing until sacrifice. The MCAO procedure, as previously described [79], involved anesthesia with 5 % enflurane, maintained with 1 %–3 % enflurane. The rat's neck skin was shaved and disinfected, followed by a longitudinal incision to expose the right CCA, external carotid artery (ECA), and internal carotid artery (ICA). After isolating the ECA's main trunk, a small opening was created in the ECA, through which a thread was inserted up to the beginning of the right MCA. The MCA was occluded for 120 min, followed by the removal of the thread to induce reperfusion. Depending on the group, either pre-sanitized 1 cm Ni-Ti or Mg wires were inserted through the ECA opening into the CCA and fixed with the ECA. We determined the implantation length of Mg wires based on the maximum length of the exposed common carotid artery which was about 1 cm. According to previous studies, a larger implantation length indicates a higher release of Mg^{2+} [41], but the protective relationship still needs further investigation. Post-surgery, the rats were sutured, returned to their cages, and provided with adequate water and food.

5.4.2. Neurological behavioral tests

Five neurological behavioral tests were conducted to assess neurological deficits in rats. Four tests, Zea-Longa scoring [79], EBST [80], rotarod test [81], and adhesive removal test [82] were performed before surgery and on days 1, 3, 5, 7, 10, and 14 post-surgery. The open field test was conducted 7 days after surgery.

Zea-Longa scoring included five levels: 0 scale, indicating no neurological deficits; 1 scale, where the left front limb could not fully extend; 2 scale, showing rotation towards the left side while walking; 3 scale, involving leaning to the left while walking; 4 scale, representing inability to walk autonomously with loss of consciousness. In the EBST, rats were lifted by their tails at the center of a 100 cm × 100 cm box. The rat's head swing to the left or right was observed. A swing angle exceeding 10° to one side was considered significant. The test concluded after 30 total swings, with the EBST score being the proportion of left swings to total swings. The rotarod test involved placing rats on an accelerating rotating rod, timing their latency to fall. Speed increased from 4 to 40 rpm within 5 min. In the adhesive removal test, the average time taken by rats to remove a piece of sticky tape from their left paw was recorded. If the tape remained after 2 min, the removal time was logged as 2 min. Lastly, the open field test involved placing each rat in the center of an open field for 5 min in a quiet room. Behavior was recorded with a video monitoring device connected to a computer (RWD Science Co., China), and the video was analyzed to calculate walking distance and time spent in different areas by the rats.

5.4.3. Infarct volume and neuron damage evaluation

Infarct volumes and neuron damage in rats were assessed 7 days post-surgery. Rats underwent transcardial perfusion with phosphate-buffered saline (PBS), followed by brain extraction. For infarct volume assessment, brains were sliced into five 2-mm sections, stained with 2 % TTC (wt/vol in PBS) for 20 min at 37 °C. The slices were photographed, and infarct volumes were calculated using Image J software as the ratio of (contralateral hemisphere area - noninfarcted area of the ipsilateral hemisphere) to contralateral hemisphere area. Neuron damage was estimated by fixing brains in 10 % formaldehyde for over 24 h. After embedding in paraffin, sectioning, and Nissl staining, the Nissl-stained sections were photographed. Nissl-positive cells were counted using Image J software. The Nissl body ratio was determined as the number of Nissl-positive cells in the ipsilateral hemisphere divided by the number in the contralateral hemisphere.

5.4.4. Brain edema and evans blue leakage

For blood-brain barrier (BBB) integrity evaluation, brain edema and Evans blue leakage were assessed 7 days after surgery. Brain edema was evaluated by measuring the wet weight of rat brains, followed by drying the tissue at 90 °C for 24 h to obtain the dry weight. Brain tissue water content percentage was calculated as (wet weight - dry weight)/wet weight × 100 %. For the Evans blue leakage test, a 2 % Evans blue dye solution (wt/vol in PBS, 3 mL/kg) was injected into the tail vein. Two hours later, rats were sacrificed via cardiac perfusion with saline. Brains were removed and photographed to assess Evans blue extravasation. Ischemic half-brain tissue was homogenized in 1 ml of formamide solution to create a cell suspension. After incubation at 60 °C for 24 h, the sample was centrifuged at 5000 rpm for 10 min. The optical density of the supernatant was measured at 635 nm with a spectrophotometer, and Evans blue content was determined using a standard curve.

5.4.5. Measurement of cerebral blood flow

Relative CBF was measured using laser speckle imaging (LSI, RWD Science Co., China), following the methodology reported previously [83]. Rats were anesthetized with 5 % enflurane, maintained with 1 %–3 % enflurane via a facemask. After shaving and disinfecting the cranium with iodophor, the rats were positioned prone and the head secured in a stereotaxic device. A longitudinal incision was made in the skin over the cranium. Using a dental drill under a dissecting microscope, the cranium from bregma to lambda was carefully thinned until CBF was clearly measurable by LSI. The mean CBF on both damaged and contralateral sides was measured, with the damaged side CBF presented as a percentage of the contralateral side's value.

5.4.6. In vivo Mg^{2+} distribution

The method for detecting released trace metals *in vivo* was based on Matusiewicz [84]. Blood from the right CCA was collected on days 1 and 7 post-implantation using a polymer needle. Subsequently, rats were sacrificed, and organs including the heart, liver, spleen, lung, kidney, ICB, and IIB were removed with Teflon-coated tweezers and ceramic scissors. The organs were weighed, placed in Teflon digestion vials, digested with HNO_3 and H_2O_2 using a microwave system, and Mg concentration was determined via ICP-OES (iCAP6300, Thermo).

5.4.7. In vivo ROS detection

Brain tissue was homogenized in a 1:10 w/v RIPA buffer. Post-homogenization, brain tissue samples were centrifuged at 12,000 rpm for 20 min at 4 °C. According to Genmed Scientifics Inc., USA, lucigenin was incubated with the supernatant. After a 15-min acclimation, luminescence was measured every second for 10 s using a luminometer (ThermoFisher Scientific, USA). Luminescence was expressed in relative light units per second.

5.4.8. In vivo Ca^{2+} detection

Following the manufacturer's instructions (Beyotime, China), Ca^{2+} content in brain tissue was determined. Initially, brain tissue was dissected into small pieces. Sample lysis solution was then added at a ratio of 1000 μl per 20 mg of tissue, and the mixture was homogenized. Subsequently, the samples were centrifuged at 10000–14000 g for 5 min at 4 °C to extract the supernatant. Finally, the supernatant was incubated with Ca^{2+} testing working solution for 10 min at room temperature. Absorbance at 575 nm was measured using an enzyme-linked immunosorbent assay, and Ca^{2+} concentration was calibrated based on the standard curve.

5.4.9. In vivo biosafety tests

Healthy rats, weighing 280–320 g, were divided into five groups. The control group received no treatment, while the other four groups were implanted with Mg wires in the right CCA for 1, 7, 14, and 28 days, respectively. Post-implantation, rats were sacrificed, and their organs (heart, liver, spleen, lung, and kidney) were extracted for histological analysis through H&E staining.

5.4.10. In vivo Mg wire degradation experiment

Mg wires were retrieved after 1, 7, 14, and 28 days of implantation, with three wires collected at each time point. They were pressure-perfused with saline to remove blood and then immersed in 2.5 % glutaraldehyde for 12 h. Subsequently, dehydration was carried out using graded ethanol (20 %, 40 %, 60 %, 80 %, 95 %, 100 %; 30 min for each grade). The Mg wires were then examined under a micro-CT scanner (Skyscan1076, Bruker) at a spatial resolution of 9 μm. Three-dimensional reconstruction of the Mg wires was conducted, and the volumes of the corrosion layer and remaining magnesium matrix were calculated using Mimics software (Mimics 10.01, Materialise Mimics®). The remaining volume of the magnesium matrix was calculated using the following formula.

$$V_R = V_{mg} \,/\, \left(V_{mg} + V_{corrosion}\right)$$

Where.

V_R is the volume proportion of the uncorroded part of the magnesium wire after being extracted
V_{mg} is the volume of the uncorroded part of the magnesium wire after being extracted
$V_{corrosion}$ is the volume of the corrosion layer volume of the magnesium wire after being extracted

After sputtering with gold, the longitudinal direction of the Mg wires was observed under SEM (S-4800 cold-cathode field-emission scanning electron microscope, Hitachi) with EDS attachment. The magnesium element content of the corrosion layer is tested by EDS surface scanning.

5.5. Hydrogen gas concentration measurements

Hydrogen gas dissolved in rat blood and Mg-immersed cell culture medium was quantitatively detected by gas chromatography (Zhejiang FULI Analytical Instrument Co., Ltd, China). For H_2 level measurement in blood, rats were pre-treated with heparin, and blood was immediately collected and injected into a 10 ml glass bottle pre-filled with fresh air. To measure H_2 levels in the medium, the medium was directly transferred into a bottle. All bottle tops were secured with a hard plastic plug and an additional screw top. The bottles were then ultrasonically treated for 30 min to ensure the release of dissolved H_2. Subsequently, the vapor was aspirated and injected into a gas chromatograph device.

5.6. Statistical analysis

All results were expressed as mean ± standard deviation. Statistical analyses were performed using SPSS 17.0. Differences between groups were analyzed using one-way ANOVA and nonparametric tests.

Conflict of interest

Authors declare that they have no competing interests.

Data availability statement

All data are available in the main text or the supplementary materials.

Ethics approval and consent to participate

The Institutional Animal Investigation Committee of Capital Medical University approved all experimental methods, ensuring that all animal treatments adhered strictly to the National Institutes of Health's guidelines for the Care and Use of Laboratory Animals.

CRediT authorship contribution statement

Yang Zhang: Writing – original draft, Visualization, Project administration, Methodology, Investigation, Conceptualization. **Hongkang Zhang:** Writing – original draft, Visualization, Project administration, Methodology, Investigation, Conceptualization. **Miaowen Jiang:** Writing – original draft, Project administration, Methodology, Conceptualization. **Xiaofeng Cao:** Project administration, Methodology. **Xiaoxiao Ge:** Investigation. **Baoying Song:** Project administration, Methodology. **Jing Lan:** Funding acquisition. **Wenhao Zhou:** Methodology. **Zhengfei Qi:** Investigation. **Xuenan Gu:** Investigation. **Juzhe Liu:** Methodology. **Yufeng Zheng:** Writing – review & editing, Supervision, Funding acquisition, Conceptualization. **Ming Li:** Writing – review & editing, Supervision, Funding acquisition, Conceptualization. **Xunming Ji:** Writing – review & editing, Supervision, Funding acquisition, Conceptualization.

Declaration of competing interest

Yufeng Zheng is the editor-in-chief for Bioactive Materials and was not involved in the editorial review or the decision to publish this article. All authors declare that they have no known competing financial interests or personal relationships that could have appeared to influence the work reported in this paper.

Acknowledgements

This study was funded by National Natural Science Foundation of China (82027802, 82102220), Research Funding on Translational Medicine from Beijing Municipal Science and Technology Commission (Z221100007422023), Beijing Hospitals Authority Clinical Medicine Development of Special Funding Support (YGLX202325), Non-profit Central Research Institute Fund of Chinese Academy of Medical (2023-JKCS-09), Beijing Association for Science and Technology Youth Talent Support Program (BYESS2022081), Science and Technology Innovation Service Capacity Building Project of Beijing Municipal Education Commission (11000023T000002157177), Outstanding Young Talents Program of Capital Medical University (B2305), Beijing Municipal Natural Science Foundation (7244510), Beijing Nova Program (20230484286).

Furthermore, we thank Beijing Tonghe Litai Biotechnology Co.Ltd for providing guidance on the operation of experimental animals.

Appendix A. Supplementary data

Supplementary data to this article can be found online at https://doi.org/10.1016/j.bioactmat.2024.08.019.

References

[1] GBD 2016 Lifetime Risk of Stroke Collaborators, Global, regional, and country-specific lifetime risks of stroke, 1990 and 2016, N. Engl. J. Med. 379 (2018) 2429–2437.
[2] F. Eren, S.E. Yilmaz, Neuroprotective approach in acute ischemic stroke: a systematic review of clinical and experimental studies, Brain circulation 8 (2022) 172–179.
[3] Y. Tong, Y. Ding, Z. Han, H. Duan, X. Geng, Optimal rehabilitation strategies for early postacute stroke recovery: an ongoing inquiry, Brain circulation 9 (2023) 201–204.
[4] C. Li, et al., Pleiotropic microenvironment remodeling micelles for cerebral ischemia-reperfusion injury therapy by inhibiting neuronal ferroptosis and glial overactivation, ACS Nano 17 (2023) 18164–18177.
[5] T. Ohta, et al., First-in-human trial of a self-expandable, temporary dilation system for intracranial atherosclerotic disease in patients presenting with acute ischemic stroke, jnis-2023-020983, J. Neurointerventional Surg. (2023).
[6] R. Xu, L. Wang, L. Sun, J. Dong, Neuroprotective effect of magnesium supplementation on cerebral ischemic diseases, Life Sci. 272 (2021) 119257.
[7] M.B. Marinov, K.S. Harbaugh, P.J. Hoopes, H.J. Pikus, R.E. Harbaugh, Neuroprotective effects of preischemia intraarterial magnesium sulfate in reversible focal cerebral ischemia, J. Neurosurg. 85 (1996) 117–124.
[8] M. Kaya, et al., The effects of magnesium sulfate on blood-brain barrier disruption caused by intracarotid injection of hyperosmolar mannitol in rats, Life Sci. 76 (2004) 201–212.
[9] I. Ohsawa, et al., Hydrogen acts as a therapeutic antioxidant by selectively reducing cytotoxic oxygen radicals, Nat. Med. 13 (2007) 688–694.
[10] H. Li, Y. Luo, P. Yang, J. Liu, Hydrogen as a complementary therapy against ischemic stroke: a review of the evidence, J. Neurol. Sci. 396 (2019) 240–246.
[11] C. Wu, et al., Molecular hydrogen: an emerging therapeutic medical gas for brain disorders, Mol. Neurobiol. 60 (2023) 1749–1765.
[12] L. Huang, C. Lenahan, W. Boling, J. Tang, J.H. Zhang, Molecular hydrogen application in stroke: bench to bedside, Curr. Pharmaceut. Des. 27 (2021) 703–712.
[13] H. Ono, et al., Hydrogen gas inhalation treatment in acute cerebral infarction: a randomized controlled clinical study on safety and neuroprotection, J. Stroke Cerebrovasc. Dis. 26 (2017) 2587–2594.
[14] H. Ono, et al., Improved brain MRI indices in the acute brain stem infarct sites treated with hydroxyl radical scavengers, Edaravone and hydrogen, as compared to Edaravone alone. A non-controlled study, Med. Gas Res. 1 (2011) 12.
[15] H. Ono, et al., A basic study on molecular hydrogen (H2) inhalation in acute cerebral ischemia patients for safety check with physiological parameters and measurement of blood H2 level, Med. Gas Res. 2 (2012) 21.
[16] K. Nagatani, et al., Safety of intravenous administration of hydrogen-enriched fluid in patients with acute cerebral ischemia: initial clinical studies, Med. Gas Res. 3 (2013) 13.
[17] G. Zhou, E. Goshi, Q. He, Micro/nanomaterials-augmented hydrogen therapy, Adv. Healthcare Mater. 8 (2019) e1900463.
[18] S. Takeuchi, K. Kumagai, T. Toyooka, N. Otani, K. Wada, K. Mori, Intravenous hydrogen therapy with intracisternal magnesium sulfate infusion in severe aneurysmal subarachnoid hemorrhage, Stroke 52 (2021) 20–27.
[19] M. Haude, et al., Safety and performance of the drug-eluting absorbable metal scaffold (DREAMS) in patients with de-novo coronary lesions: 12 month results of the prospective, multicentre, first-in-man BIOSOLVE-I trial, Lancet 381 (2013) 836–844.
[20] M. Haude, et al., Safety and performance of the second-generation drug-eluting absorbable metal scaffold in patients with de-novo coronary artery lesions (BIOSOLVE-II): 6 month results of a prospective, multicentre, non-randomised, first-in-man trial, Lancet 387 (2016) 31–39.
[21] J. Zhang, et al., The degradation and transport mechanism of a Mg-Nd-Zn-Zr stent in rabbit common carotid artery: a 20-month study, Acta Biomater. 69 (2018) 372–384.
[22] A. Sato, et al., Initial organ distribution and biological safety of Mg2+ released from a Mg alloy implant, Biomed. Mater. (2018) 035006.
[23] Q. Long, X.Y. Xu, K.V. Ramnarine, P. Hoskins, Numerical investigation of physiologically realistic pulsatile flow through arterial stenosis, J. Biomech. 34 (2001) 1229–1242.
[24] S. Zhang, et al., Research on an Mg-Zn alloy as a degradable biomaterial, Acta Biomater. 6 (2010) 626–640.
[25] T. Sakai, et al., Consumption of water containing over 3.5 mg of dissolved hydrogen could improve vascular endothelial function, Vasc. Health Risk Manag. 10 (2014) 591–597.
[26] P. Georgoff, et al., Hydrogen-1 MR spectroscopy for measurement and diagnosis of hepatic steatosis, AJR Am. J. Roentgenol. 199 (2012) 2–7.
[27] U. Riaz, I. Shabib, W. Haider, The current trends of Mg alloys in biomedical applications-A review, J. Biomed. Mater. Res. B Appl. Biomater. 107 (2019) 1970–1996.
[28] Z.Q. Zhang, Y.X. Yang, J.A. Li, R.C. Zeng, S.K. Guan, Advances in coatings on magnesium alloys for cardiovascular stents - a review, Bioact. Mater. 6 (2021) 4729–4757.
[29] Y. Xing, G. Liang, T. Zhu, Current status and outlook of potential applications of biodegradable materials in cerebral vascular stents, Neurosurg. Rev. 45 (2022) 3565–3571.
[30] M. Li, et al., Current status and outlook of biodegradable metals in neuroscience and their potential applications as cerebral vascular stent materials, Bioact. Mater. 11 (2022) 140–153.
[31] J. Zhang, B. Zhang, J. Zhang, W. Lin, S. Zhang, Magnesium promotes the regeneration of the peripheral nerve, Front. Cell Dev. Biol. 9 (2021) 717854.
[32] W. Daly, L. Yao, D. Zeugolis, A. Windebank, A. Pandit, A biomaterials approach to peripheral nerve regeneration: bridging the peripheral nerve gap and enhancing functional recovery, J. R. Soc. Interface 9 (2012) 202–221.
[33] J.Z. Fan, V. Lopez-Rivera, S.A. Sheth, Over the horizon: the present and future of endovascular neural recording and stimulation, Front. Neurosci. 14 (2020) 432.
[34] S. Chatterjee, M. Saxena, D. Padmanabhan, M. Jayachandra, H.J. Pandya, Futuristic medical implants using bioresorbable materials and devices, Biosens. Bioelectron. 142 (2019) 111489.
[35] B.E. Grüter, et al., Testing bioresorbable stent feasibility in a rat aneurysm model, J. Neurointerventional Surg. 11 (2019) 1050–1054.
[36] W. Wang, et al., Magnesium alloy covered stent for treatment of a lateral aneurysm model in rabbit common carotid artery: an in vivo study, Sci. Rep. 6 (2016) 37401.
[37] J.B. Zong, Q.W. He, Y.X. Liu, M. Qiu, J.H. Wu, B. Hu, Advances in the development of biodegradable coronary stents: a translational perspective, Materials Today Bio 16 (2022).
[38] J. Wang, et al., Flow-induced corrosion of absorbable magnesium alloy: in-situ and real-time electrochemical study, Corrosion Sci. 104 (2016) 277–289.
[39] J. Wang, C.E. Smith, J. Sankar, Y. Yun, N. Huang, Absorbable magnesium-based stent: physiological factors to consider for in vitro degradation assessments, Regen Biomater 2 (2015) 59–69.

[40] X. Zhao, M. Zhao, S. Amin-Hanjani, X. Du, S. Ruland, F.T. Charbel, Wall shear stress in major cerebral arteries as a function of age and gender–a study of 301 healthy volunteers, J. Neuroimaging 25 (2015) 403–407.
[41] C. Wu, et al., Molecular hydrogen: an emerging therapeutic medical gas for brain disorders, Mol. Neurobiol. 60 (2023) 1749–1765.
[42] C.P. Derdeyn, et al., Aggressive medical treatment with or without stenting in high-risk patients with intracranial artery stenosis (SAMMPRIS): the final results of a randomised trial, Lancet 383 (2014) 333–341.
[43] P. Gao, et al., Effect of stenting plus medical therapy vs medical therapy alone on risk of stroke and death in patients with symptomatic intracranial stenosis: the CASSISS randomized clinical trial, JAMA 328 (2022) 534–542.
[44] Q. Zhang, M. Jia, Y. Wang, Q. Wang, J. Wu, Cell death mechanisms in cerebral ischemia-reperfusion injury, Neurochem. Res. 47 (2022) 3525–3542.
[45] P.B.L. Pun, J. Lu, S. Moochhala, Involvement of ROS in BBB dysfunction, Free Radic. Res. 43 (2009) 348–364.
[46] Y. Zhang, et al., "No-reflow" phenomenon in acute ischemic stroke, J. Cerebr. Blood Flow Metabol. 271678X231208476 (2023).
[47] V.E. O'Collins, M.R. Macleod, G.A. Donnan, L.L. Horky, B.H. van der Worp, D. W. Howells, 1,026 experimental treatments in acute stroke, Ann. Neurol. 59 (2006) 467–477.
[48] R.L. Dedrick, Arterial drug infusion: pharmacokinetic problems and pitfalls, J. Natl. Cancer Inst. 80 (1988) 84–89.
[49] K. Nagatani, et al., Effect of hydrogen gas on the survival rate of mice following global cerebral ischemia, Shock 37 (2012) 645–652.
[50] X. Wu, et al., Hydrogen exerts neuroprotective effects on OGD/R damaged neurons in rat hippocampal by protecting mitochondrial function via regulating mitophagy mediated by PINK1/Parkin signaling pathway, Brain Res. 1698 (2018) 89–98.
[51] Y. Yan, C. Wei, W. Zhang, H. Cheng, J. Liu, Cross-talk between calcium and reactive oxygen species signaling, Acta Pharmacol. Sin. 27 (2006) 821–826.
[52] M. Yemisci, Y. Gursoy-Ozdemir, A. Vural, A. Can, K. Topalkara, T. Dalkara, Pericyte contraction induced by oxidative-nitrative stress impairs capillary reflow despite successful opening of an occluded cerebral artery, Nat. Med. 15 (2009) 1031–1037.
[53] C.N. Hall, et al., Capillary pericytes regulate cerebral blood flow in health and disease, Nature 508 (2014) 55–60.
[54] T. Westermaier, E. Hungerhuber, S. Zausinger, A. Baethmann, R. Schmid-Elsaesser, Neuroprotective efficacy of intra-arterial and intravenous magnesium sulfate in a rat model of transient focal cerebral ischemia, Acta Neurochir. 145 (2003).
[55] I. Harakawa, T. Yano, T. Sakurai, N. Nishikimi, Y. Nimura, Measurement of spinal cord blood flow by an inhalation method and intraarterial injection of hydrogen gas, J. Vasc. Surg. 26 (1997) 623–628.
[56] J. Liu, et al., Comparative in vitro study on binary Mg-RE (Sc, Y, La, Ce, Pr, Nd, Sm, Eu, Gd, Tb, Dy, Ho, Er, Tm, Yb and Lu) alloy systems, Acta Biomater. 102 (2020) 508–528.
[57] X. Gu, Y. Zheng, Y. Cheng, S. Zhong, T. Xi, In vitro corrosion and biocompatibility of binary magnesium alloys, Biomaterials 30 (2009) 484–498.
[58] Y. Zhang, et al., Implant-derived magnesium induces local neuronal production of CGRP to improve bone-fracture healing in rats, Nat. Med. 22 (2016) 1160–1169.
[59] X. Jiang, et al., Effect of Mg-Zn-Nd-Zr magnesium alloy on the activity and differentiation of neural cells, J Int Nuerol and Neurosurg 48 (2021) 343–348.
[60] J. Xie, et al., Magnesium oxide/poly(l-lactide-co-ε-caprolactone) scaffolds loaded with neural morphogens promote spinal cord repair through targeting the calcium influx and neuronal differentiation of neural stem cells, Adv. Healthcare Mater. 11 (2022) e2200386.
[61] S. Jia, et al., Elevation of brain magnesium potentiates neural stem cell proliferation in the Hippocampus of Young and aged mice, J. Cell. Physiol. 231 (2016) 1903–1912.
[62] T.L.P. Slottow, et al., Optical coherence tomography and intravascular ultrasound imaging of bioabsorbable magnesium stent degradation in porcine coronary arteries, Cardiovasc. Revascularization Med. 9 (2008) 248–254.
[63] R. Erbel, et al., Temporary scaffolding of coronary arteries with bioabsorbable magnesium stents: a prospective, non-randomised multicentre trial, Lancet 369 (2007) 1869–1875.
[64] N. Yang, et al., Magnesium galvanic cells produce hydrogen and modulate the tumor microenvironment to inhibit cancer growth, Nat. Commun. 13 (2022) 2336.
[65] B. Liu, et al., Zn-Fe primary battery-enabled controlled hydrogen release in stomach for improving insulin resistance in obesity-associated type 2 diabetes, Bioact. Mater. 33 (2024) 242–250.
[66] W. Wan, et al., An in situ depot for continuous evolution of gaseous H2 mediated by a magnesium passivation/activation cycle for treating osteoarthritis, Angew Chem. Int. Ed. Engl. 57 (2018) 9875–9879.
[67] S. Chen, et al., Interaction between cerebral small vessel disease, blood pressure, and remote ischemic lesions in acute spontaneous intracerebral hemorrhage, Eur Stroke J 8 (2023) 828–835.
[68] Z. Peng, et al., Biomaterial based implants caused remote liver fatty deposition through activated blood-derived macrophages, Biomaterials 301 (2023) 122234.
[69] C. Hou, et al., Chronic remote ischaemic conditioning in patients with symptomatic intracranial atherosclerotic stenosis (the RICA trial): a multicentre, randomised, double-blind sham-controlled trial in China, Lancet Neurol. 21 (2022) 1089–1098.
[70] R.A. Blauenfeldt, et al., Remote ischemic conditioning for acute stroke: the RESIST randomized clinical trial, JAMA 330 (2023) 1236–1246.
[71] H. Chen, et al., Effect of remote ischemic conditioning vs usual Care on neurologic function in patients with acute moderate ischemic stroke: the RICAMIS randomized clinical trial, JAMA 328 (2022) 627–636.
[72] Z. Li, S.J. Zhou, N. Huang, Effects of ECAE processing temperature on the microstructure, mechanical properties, and corrosion behavior of pure Mg, Int. J. Miner. Metall. Mater. 22 (2015) 639–647.
[73] S. Feng, et al., Edaravone for acute ischaemic stroke, Cochrane Database Syst. Rev. CD007230 (2011).
[74] S. Wang, et al., Dl-3-n-Butylphthalide (NBP): a promising therapeutic agent for ischemic stroke, CNS Neurol. Disord.: Drug Targets 17 (2018) 338–347.
[75] M.P. Bonaca, N.M. Hamburg, M.A. Creager, Contemporary medical management of peripheral artery disease, Circ. Res. 128 (2021) 1868–1884.
[76] J. Claassen, S. Park, Spontaneous subarachnoid haemorrhage, Lancet 400 (2022) 846–862.
[77] B.A. Gross, K.U. Frerichs, Stent usage in the treatment of intracranial aneurysms: past, present and future, J. Neurol. Neurosurg. Psychiatry 84 (2013) 244–253.
[78] M.G. Nasoni, et al., Melatonin reshapes the mitochondrial network and promotes intercellular mitochondrial transfer via tunneling nanotubes after ischemic-like injury in hippocampal HT22 cells, J. Pineal Res. 71 (2021) e12747.
[79] E.Z. Longa, P.R. Weinstein, S. Carlson, R. Cummins, Reversible middle cerebral artery occlusion without craniectomy in rats, Stroke 20 (1989) 84–91.
[80] C.V. Borlongan, P.R. Sanberg, Elevated body swing test: a new behavioral parameter for rats with 6-hydroxydopamine-induced hemiparkinsonism, J. Neurosci. 15 (1995) 5372–5378.
[81] D.C. Rogers, C.A. Campbell, J.L. Stretton, K.B. Mackay, Correlation between motor impairment and infarct volume after permanent and transient middle cerebral artery occlusion in the rat, Stroke 28 (1997).
[82] J. Chen, et al., Therapeutic benefit of intravenous administration of bone marrow stromal cells after cerebral ischemia in rats, Stroke 32 (2001) 1005–1011.
[83] L.A. Allen, M. Terashvili, A. Gifford, J.H. Lombard, Evaluation of cerebral blood flow autoregulation in the rat using laser Doppler flowmetry, J. Vis. Exp. (2020).
[84] H. Matusiewicz, Potential release of in vivo trace metals from metallic medical implants in the human body: from ions to nanoparticles–a systematic analytical review, Acta Biomater. 10 (2014) 2379–2403.